Striatal origin of the pathologic beta oscillations in Parkinson's disease

M. M. McCarthy[a,1], C. Moore-Kochlacs[a,2], X. Gu[b,2], E. S. Boyden[c], X. Han[b], and N. Kopell[a,1]

[a]Department of Mathematics and Statistics, Boston University, Boston, MA 02215; [b]Department of Biomedical Engineering, Photonics Center, Boston University, Boston, MA 02215; and [c]Media Lab, Massachusetts Institute of Technology, Cambridge, MA 02139

Contributed by N. Kopell, May 17, 2011 (sent for review December 28, 2010)

Enhanced oscillations at beta frequencies (8–30 Hz) are a signature neural dynamic pathology in the basal ganglia and cortex of Parkinson's disease patients. The mechanisms underlying these pathological beta oscillations remain elusive. Here, using mathematical models, we find that robust beta oscillations can emerge from inhibitory interactions between striatal medium spiny neurons. The interaction of the synaptic GABAa currents and the intrinsic membrane M-current promotes population oscillations in the beta frequency range. Increased levels of cholinergic drive, a condition relevant to the parkinsonian striatum, lead to enhanced beta oscillations in the striatal model. We show experimentally that direct infusion of the cholinergic agonist carbachol into the striatum, but not into the neighboring cortex, of the awake, normal rodent induces prominent beta frequency oscillations in the local field potential. These results provide evidence for amplification of normal striatal network dynamics as a mechanism responsible for the enhanced beta frequency oscillations in Parkinson's disease.

computational model | acetylcholine | muscarinic | mouse

Enhanced beta frequency oscillations are correlated with bradykinesia, a disabling movement abnormality in Parkinson's disease patients (1). Improvement of bradykinesia correlates with a decrease in the enhanced beta frequency oscillations in the subthalamic nucleus (STN) and cortex of Parkinson's disease patients (2). However, the function of the beta oscillations in parkinsonian pathology remains elusive, and the source of these oscillations is unknown. Two predominating theories exist about the origin of these enhanced beta rhythms. One hypothesis proposes that oscillations arise from the interaction of the STN and the external segment of the globus pallidus (GPe); this is known as the STN/GPe pacemaker hypothesis (3). Evidence for the STN/GPe pacemaker hypothesis comes from a study showing that GPe and STN are able to generate synchronized oscillatory bursting activity in the range of 0.4–1.8 Hz in organotypic cultures of cortex-striatum-STN-GPe (4). A second theory of beta generation in Parkinson's disease entails cortical patterning of the STN (3). This theory derives partly from studies on anesthetized rats showing that, with dopamine depletion, oscillatory spiking activity in STN and GPe is correlated with and largely dependent on cortical slow-wave (~1 Hz) activity (5). For the cortical patterning, but not the STN/GPe hypothesis, there is experimental evidence for intrinsic production of the beta rhythm (6).

Degeneration of dopaminergic neurons that project to the striatum is a hallmark of Parkinson's disease pathology (7), but the striatum has been largely ignored as a possible source of beta frequency rhythms in Parkinson's disease. There are several reasons for ignoring the striatum. The striatum consists of an almost entirely inhibitory network of cells (99.7% are GABAergic and 0.3% are cholinergic in the rat neostriatum) (8). Furthermore, the predominant striatal cell type, the medium spiny neuron (MSN), rarely spikes (average rate of 1.1 ± 0.18 Hz in freely moving rats) (9). It is not evident that this largely inactive and inhibitory network can generate any independent activity, much less rhythmic activity at a relatively high frequency (8–30 Hz). However, mathematical modeling informs us that inhibition can create neuronal excitation under certain conditions. Specifically, the activation or inactivation of slow currents can lead to the phenomenon of postinhibitory rebound spiking. Moreover, inhibitory networks of such neurons can produce rhythmic activity (10, 11). The frequency of the rhythm largely depends on the time constant of the slow current. At least one slow current is known to have a time constant of decay that allows postinhibitory rebound spiking to occur with a lag appropriate for the formation of beta frequency spiking: the M-current (10). The M-current is a noninactivating potassium current, and GABAa inhibition can temporarily reduce this current, leaving the neuronal membrane in a more excited state (12). The MSNs of the striatum have an M-current and receive inhibition from each other through GABAa synapses. Therefore, the MSNs of the striatum contain both the cellular and the network properties to support the generation of beta frequency oscillations.

We construct mathematical models of networks of MSNs and find that such networks are capable of generating robust beta oscillations. Perturbations that enhance the interaction between MSN M-current and GABAa current increase the power of the population beta rhythm. An interesting prediction is that increases in either MSN background excitation (I_{app}) or MSN GABAergic inhibition will increase the power of beta oscillations in the model MSN network. Because increasing MSN excitation necessarily increases MSN to MSN inhibition, these seemingly opposite effects, in fact, work synergistically to create beta frequency oscillations in our model MSN networks.

Striatopallidal MSNs have high levels of dopamine D2 receptors and increase their excitability in response to loss of dopamine (13). Furthermore, loss of dopamine has been shown to increase beta oscillations in striatum (14). This finding is consistent with our model results, which predict enhanced beta oscillations in the subnetwork of striatopallidal MSNs after loss of striatal dopamine. MSN excitability can also be increased by other neuromodulators, most notably by the action of acetylcholine (ACh) on M1 receptors (13). This is important in the context of Parkinson's disease, because dopamine modulates ACh levels. Dopamine tonically inhibits ACh release in the striatum under normal physiological conditions by its action on D2 receptors (15). Moreover, antagonists of either D1 or D2 receptors as well as loss of striatal dopamine in the 6-hydroxydopamine (6-OHDA) rat, an animal model of Parkinson's disease, result in increased striatal levels of ACh (16).

As a first test of our model, we inject the muscarinic acetylcholine receptor agonist carbachol into the striatum of normal awake mice. As predicted, cholinergic agonists in the striatum induce enhanced beta frequency oscillations in the striatal local field potential (LFP). Neither striatal nor cortical LFPs show

Author contributions: M.M., E.S.B., X.H., and N.K. designed research; M.M., C.M.-K., X.G., and X.H. performed research; M.M., C.M.-K., X.G., and X.H. analyzed data; and M.M., E.S.B., X.H., and N.K. wrote the paper.

The authors declare no conflict of interest.

[1]To whom correspondence may be addressed. E-mail: mmccart@bu.edu or nk@bu.edu.

[2]C.M.-K. and X.G. contributed equally to this work.

This article contains supporting information online at www.pnas.org/lookup/suppl/doi:10.1073/pnas.1107748108/-/DCSupplemental.

increased beta oscillations after infusion of carbachol into the cortex, showing that striatal LFP beta is not the result of diffusion of carbachol into the neighboring cortex. Our combined computational and experimental results suggest that increased MSN excitation, which produces increased MSN to MSN inhibitory interactions, is a potential source of the enhanced beta rhythms in Parkinson's disease. Our modeling results also suggest that loss of dopamine and increased striatal ACh work in parallel to amplify beta oscillations in striatal networks in Parkinson's disease.

Results from Mathematical Models of Normal and Parkinsonian Networks of MSNs

Networks of MSNs Alone Produce Beta Oscillations. A raster plot of our 100-neuron striatal model (see *Computational Methods*) using weak all-to-all connections displays no readily observable pattern of activity among MSNs (Fig. 1*A*). However, analysis of the model LFP reveals a distinct peak in the low beta frequency range centered around 12.1 ± 0.7 Hz (Fig. 1*B*). The beta frequency oscillations wax and wane over time (Fig. 1*C*). The spiking of individual MSNs is irregular (Fig. 1*D*). The average spiking rate of the neurons in this network is 0.96 ± 0.03 Hz, consistent with the low average MSN spiking rate in vivo (9). The trace of the model LFP also contains waxing and waning beta frequency oscillations (Fig. 1*E*).

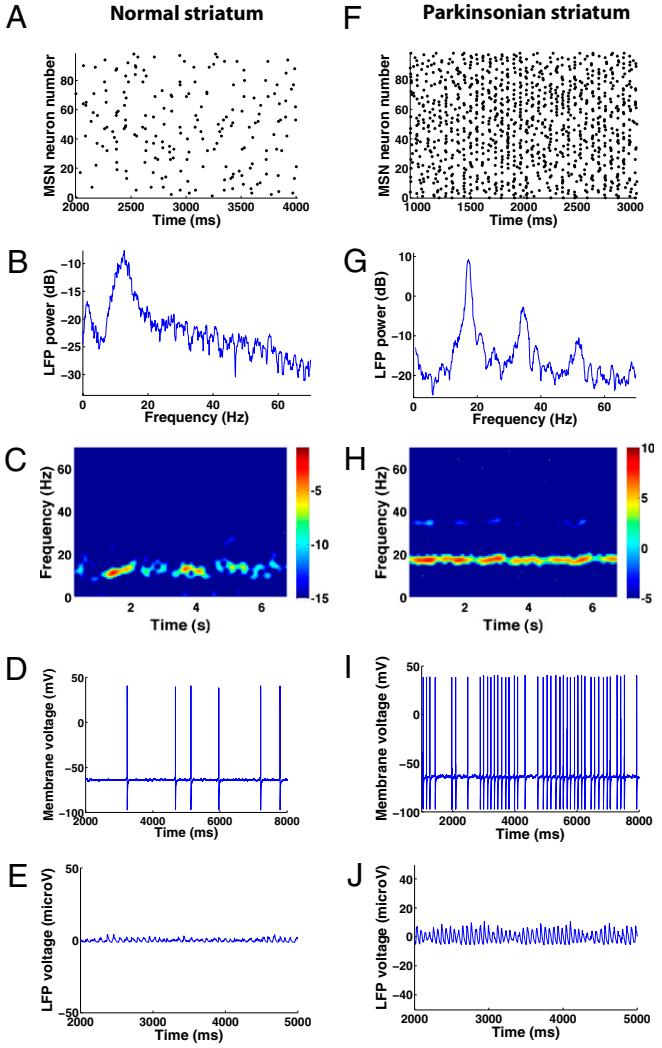

Fig. 1. Beta oscillations emerge in the model striatum under normal conditions and become enhanced under parkinsonian conditions. *A–E* are taken from the same 7-s simulation under normal conditions, and *F–J* are from the same 7-s simulation under parkinsonian conditions. (*A*) Raster plot of 100 reciprocally connected medium spiking neurons (MSNs) under normal, non-parkinsonian conditions. (*B*) Power spectral density of the model LFP. (*C*) Spectrogram of the model LFP. (*D*) Membrane voltage fluctuations from one MSN in the network. (*E*) Waxing and waning of the model LFP trace under normal conditions. (*F*) Raster plot of 100 reciprocally connected MSNs under parkinsonian conditions. (*G*) Power spectral density of the model LFP. (*H*) Spectrogram of the model LFP. (*I*) Membrane voltage fluctuations from one MSN in the parkinsonian network. (*J*) The model LFP trace under parkinsonian conditions.

Beta Power and MSN Spiking Frequency Increase in Parkinson's Disease Model Striatum. We simulate the loss of dopamine in the parkinsonian striatum indirectly through ACh-induced reduction of the M-current (see *Computational Methods*). Decreasing the maximal M-current conductance by 7.7% has pronounced effects on the striatal network dynamics [the percent decrease of the maximal M-current conductance ($\bar{g}_m$) depends on various parameters; for example, Fig. S1 shows a qualitatively similar model in which the M-current changes 41.2% between the normal and parkinsonian states]. MSN spiking becomes more obviously patterned into a beta frequency population rhythm (Fig. 1*F*). The LFP power peaks at a higher frequency (17.1 ± 0.32 Hz), and the peak power is higher than in the non-parkinsonian condition (Fig. 1*G*). This beta oscillation is persistent in contrast to the waxing and waning of the oscillation in the non-parkinsonian condition (Fig. 1*H*). Individual MSNs show more prominent subthreshold beta frequency oscillations because of the increased number of MSNs participating in the population beta rhythm, which provides individual MSNs with increased beta frequency synaptic input (Fig. 1*I*). MSNs spike more frequently than in the non-parkinsonian condition, with an average spiking rate of 4.9 ± 0.15 Hz. The animal literature is unclear; some studies show an increase in striatal activity with parkinsonism (9, 17), whereas others show a decrease (18). The model LFP contains a more pronounced and persistent oscillatory component in the beta frequency range (Fig. 1*J*). We note that the exact frequency range of oscillations found experimentally within the basal ganglia differs among papers; some describe 15–30 Hz oscillations, whereas others extend this range down to 8 Hz (19, 20).

Properties of the Mathematical Model

GABAa-Current and M-Current Conductance Strengths and Background Excitation (I_{app}) Modulate LFP Beta Power and Peak Beta Frequency. Here, we are not looking at normal and parkinsonian states but merely at the change in beta as we change a parameter. The power and frequency of the beta oscillation tend to change nonmonotonically as the GABAa conductance is increased. (Fig. S2 and Fig. S3 *A* and *B*). Decreasing the M-current conductance or increasing I_{app} tends to increase both the power and frequency of the beta oscillation (Fig. S3 *C–F*). In the absence of M-current, the MSN neurons resemble fast-spiking (FS) interneurons. We find that it is possible to obtain beta oscillations in networks of striatal FS interneurons alone but not in a regime supported by the experimental literature (Fig. S4).

Model Results Are Largely Invariant to Changes in Network Connectivity, Network Size, and Heterogeneity. Model striatal networks with either nearest neighbor connections or random network connections give qualitatively similar results to the network with all-to-all connections (*SI Note 4: Model results are largely invariant to changes in network connectivity, network size, and heterogeneity*; Fig. S5*A*). Increasing the number of MSNs to 400 or introducing heterogeneity by giving individual MSNs different maximal GABAa conductances leads to qualitatively similar behavior to the networks with 100 MSNs and homogeneous maximal GABAa conductances. Heterogeneity also helps us distinguish between the models of MSNs with and without M-current, because

MSNs without M-current are not robust to heterogeneity. Additional information is in *SI Note 4: Model results are largely invariant to changes in network connectivity, network size, and heterogeneity*; Fig. S5*B* and Fig. S6.

Experimental Results

Increase in Striatal Cholinergic Activity Leads to Increase in Striatal Beta Frequency Oscillations. We tested our model experimentally by recording the striatal LFP while infusing the cholinergic agonist carbachol into the striatum of normal awake, head-fixed mice. Carbachol (0.5–1 mM and 1–2 μL) infusion directly into the dorsolateral striatum (stereotactic coordinate: AP (anterior posterior) = −0.2 to 0.8, ML (medial lateral) = 2.0–2.5, and DV (dorsal ventral) = 3.0–3.5) induced prominent beta frequency oscillations in simultaneously recorded LFP (Fig. 2 *A*–*E*). Often, the observed increase in beta power was preceded with a brief decrease in beta power (Fig. 2*A*). Episodes of prominent increase in beta oscillations often last several hundred milliseconds to several seconds, and they often presented a slight decrease in frequencies from high to low beta during each episode (Fig. 2 *D* and *E*). Upon striatal carbachol infusion, a tremor-like movement was observed on the contralateral side. We refer to this movement as tremor-like to indicate that the movement has a rhythmic component. We do not assume that these movements represent the parkinsonian tremor, which occurs at a higher frequency. These tremor-like movements often interrupt the enhanced beta oscillation episodes before each movement onset. This observation is consistent with evidence that desynchronization of beta frequency oscillations occurs in both non-Parkinson's and Parkinson's disease patients before movement, although the latency to premovement desynchronization is delayed in Parkinson's disease patients in the absence of L-dopa (21–23).

Of the six mice tested, it took 442 ± 119 ms (mean ± SD) for beta power to increase after infusion onset. Because the infusion site is typically positioned 300–700 μm away from the recording electrode, diffusion of carbachol from the infusion site to the recording electrode may account for a significant portion of this observed delay. After the increase in beta power, beta power often dropped below the baseline and stayed low for an extended period even at the end of the recording session, typically 1 h after the end of infusion (Fig. 2*F*).

To eliminate the possibility that the observed LFP change was caused by the pressure induced by drug infusion, which may activate mechano-sensitive mechanisms in the striatum, we infused carbachol at a lower concentration (0.1–0.2 mM, $n = 5$; three mice infused with 1–2 μL and two mice infused with 4–5 μL). Infusion of low-concentration carbachol failed to induce any change in the LFP, even with up to 5 μL infusion. Beta power remained stable throughout the entire infusion period (Fig. 2*G*). Furthermore, we did not observe any reduction in beta power at the end of these recording sessions. Thus, the reduction in beta oscillations following augmentation as induced with high-concentration carbachol infusion cannot be explained by prolonged recording, confirming that the observed beta power reduction following beta increase is due to neural network mechanisms (Fig. 2*F*). In addition, in mice infused with low-concentration carbachol, no prominent tremor-like movement was observed.

Striatum Contains Sufficient Neural Network Components to Initiate Enhanced Beta Oscillations upon Cholinergic Activation. To examine whether the observed increase in beta oscillations is initiated in the striatum but not due to the diffusion of carbachol into the adjacent cortical regions, we infused carbachol (1 mM) into the cortex directly above the dorsolateral striatum where the striatal

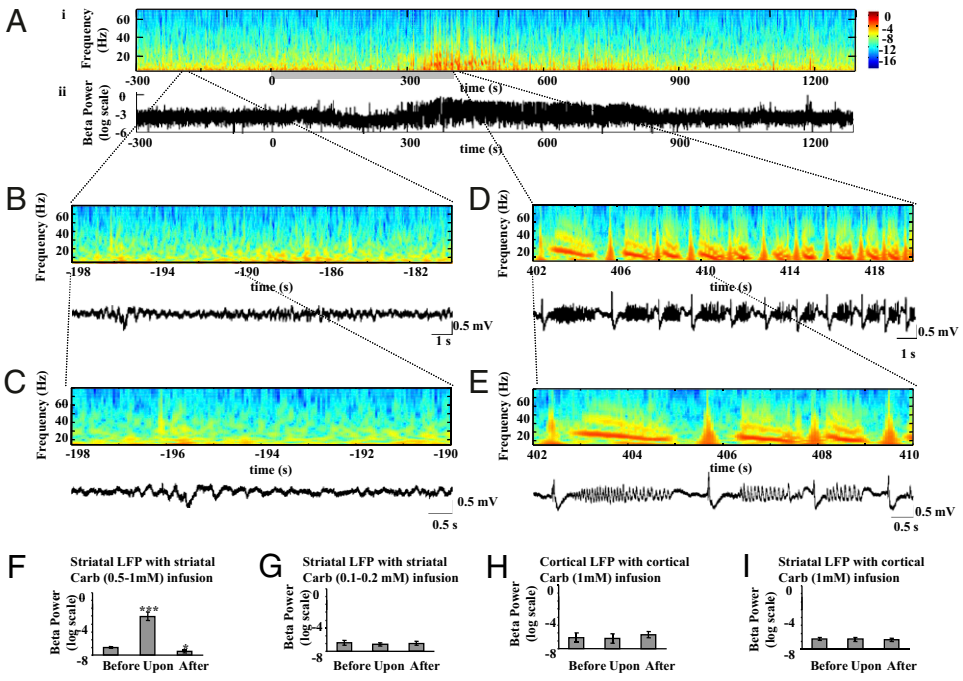

Fig. 2. Enhanced beta oscillations emerge in striatal LFP after carbachol infusion. (*A*) Power spectrum of the LFP recorded in the striatum of an awake, head-fixed mouse before, during, and after striatal carbachol infusion. (*Upper*) LFP power spectrum at 3–70 Hz on a log scale. (*Lower*) LFP power at beta frequency (10–30 Hz). (*B* and *C*) Power spectrum and LFP during a representative time window before carbachol infusion. (*Upper*) Power spectrum. (*Lower*) Corresponding LFP recorded in the striatum. (*D* and *E*) Power spectrum and LFP during a representative time window upon carbachol infusion. (*Upper*) Power spectrum. (*Lower*) Corresponding LFP recorded in the striatum. (*F*) Beta frequency power of the LFP recorded in the striatum before, during, and after carbachol (0.5–1.0 mM) infusion in the striatum ($n = 6$ mice; $^{***}P < 0.005$ and $^{*}P < 0.05$ paired t test compared to the power before carbachol infusion). (*G*) Beta frequency power of LFP recorded in the striatum before, during, and after low concentration carbachol (0.1–0.2 mM) infusion in the striatum ($n = 5$ mice). (*H*) Beta frequency power of LFP recorded in the cortex before, during, and after carbachol (1 mM) infusion in the cortex ($n = 5$ mice). (*I*) Beta frequency power of LFP recorded in the striatum before, during, and after carbachol (1 mM) infusion in the cortex ($n = 5$ mice).

infusion sites were located. We did not observe any increase in beta oscillations either locally in the cortex adjacent to the cortical infusion site or in the striatum directly below (Fig. 2 *H* and *I*). When advancing the infusion apparatus into the dorsolateral striatum and infusing carbachol (1 mM) in the striatal sites, we reliably induced an increase in beta oscillations in the striatum, confirming that the lack of beta increase on infusion in the cortical areas is due to the local network properties at the cortical infusion sites. These results demonstrate that carbachol diffusion into the cortical regions cannot explain the increase in striatal beta oscillations upon striatal infusion, thus suggesting that striatum is sufficient to induce enhanced beta oscillations.

Discussion

Our results indicate that the interaction between the MSN GABAa current and the M-current generates beta frequency oscillations within striatal networks of MSNs. Increased MSN excitation promotes additional cellular-level interaction between these two currents, resulting in increased beta frequency power in the model LFP. Our experimental work verifies that increasing MSN excitability through amplification of striatal cholinergic tone, a condition relevant to Parkinson's disease, is sufficient to engender robust beta frequency rhythms in the striatum.

Although it is not surprising that a muscarinic agonist may increase MSN spiking rate (13), it is surprising that a muscarinic agonist can induce rhythmic activity in the beta frequency range in striatum. Our mathematical model of striatum predicts that the M-current plays an important role in establishing the beta frequency of the rhythm. The mechanism by which reciprocally connected GABAergic neurons with an M-current generate beta frequency population spiking is described in McCarthy et al. (10). The GABAa current reduces the M-current by bringing the membrane potential closer to the potassium reversal potential. Reduction of the M-current depolarizes the neuron, potentially allowing the neuron to rebound spike. The dynamical interaction involving the slow time constants of decay of each current allows rebound spiking to occur with lags appropriate to the formation of a beta rhythm. An unintuitive consequence of this interaction is that increasing the GABAa conductance can cause a greater reduction of the M-current and provide additional membrane excitation. As a result of increasing GABAa conductance, the neuron may be able to rebound spike in situations that otherwise it would not, thus allowing greater participation of neurons in the network behavior. This mechanism of GABAa potentiation-induced increase in membrane excitation is explained in more detail in Fig. S7. The production of beta rhythms in the context of low individual neuronal spiking rates and noise is discussed in *SI Note 6*: *Noise*. The mechanism of striatal beta rhythm production that we propose is dependent on the reversal potential of GABAa being low (around −80 mV) such that the GABAa reversal potential is close enough to the potassium reversal potential to cause suppression of the M-current when GABAa is activated. This is supported by findings of the MSN inhibitory postsynaptic current reversal potential around −76 mV (24), although other studies report a more positive reversal potential (−62 and −64 mV) (25, 26) (see *SI Note 7*: *Reversal Potentials*). Our study suggests that the striatum contains the necessary neural network components to augment beta oscillations upon excitation of MSNs and that network interactions between MSNs alone, independent of striatal GABAergic interneurons, may be capable of creating beta frequency oscillations. Furthermore, the ability of our model to produce beta and to increase that beta in the parkinsonian state are both largely invariant to the pattern of network connectivity. This is an important result, suggesting that the beta rhythms in striatum may be quite robust to plastic changes in network connectivity.

Because MSN to MSN connections are very weak, their function in the striatal network is unclear (24). Our results here suggest that these weak connections structure the spiking of MSNs so that the latter is more likely to spike at the same phase of the beta cycle. Furthermore, any modulator of the GABAa current will influence the magnitude and peak frequency of the MSN network beta oscillation. Increasing the GABAa conductance increases the peak frequency of the beta oscillation. Because elevated MSN spiking rates increase MSN to MSN GABAergic inhibition, any potentiator of MSN excitability increases the beta frequency oscillation in our model MSN network. Thus, the weak GABAa synapses between MSNs generate a highly modulable system in which both the power and the frequency of the beta oscillations are regulated by modulators of either MSN excitability or the GABAa current. Although the functional physiological significance of both normal and pathological beta rhythms remains to be elucidated, a high degree of modulation provides this system with the flexibility to adapt to a range of behavioral conditions. Additional study of this system will reveal the extent to which modulators of GABAa and the M-current can create beta rhythms in the MSN (*SI Note 8: Other currents in MSNs* has more discussion of this topic).

Our models predict increased MSN spiking in the parkinsonian state. Such increased spiking activity of MSNs has been reported in animal models of Parkinson's disease (9, 27). Our models also predict an increased number of MSNs spiking at the same phase of each cycle of the beta rhythm under parkinsonian conditions. Because MSNs are the only output neurons of the striatum, increasing the number of synchronously spiking MSNs at each cycle of the beta oscillation has important implications concerning the transmission of this rhythmicity to downstream structures. Substantial convergence of input is thought to occur between the striatum and the globus pallidus (GP) because of the much larger number of neurons in striatum compared with the GP (28). Thus, increasing MSN synchrony should lead to stronger GABAergic input onto GP neurons. Because GP neurons can phase reset in response to GABAa inhibitory input (29) and in particular, to transient striatal input (30), the GP neurons receiving the synchronous MSN input may be patterned into the beta frequency oscillation. Additionally, in Parkinson's disease, D1 and D2 MSNs are thought to decrease and increase their excitability, respectively, in response to loss of dopamine (13, 31). Our model predicts the power of the beta oscillation scales with the level of excitation in the MSN population. Thus, we expect the population of D2 MSNs to increase network beta in the parkinsonian state and the population of D1 MSNs to decrease network beta in the parkinsonian state. Furthermore, because the rate of unilateral connectivity from D1 to D2 MSNs is relatively low (6%) (32), we do not expect significant interaction between these populations. Thus, we expect the mechanism of beta rhythm production that we describe here to be most applicable to the dynamics of neurons that project mainly to GPe (D2 MSNs) in the context of Parkinson's disease. This is in line with current thinking that suggests that the direct pathway is underactive in Parkinson's disease and that the indirect pathway is overactive (1).

Our computational model producing striatal beta oscillations is independent of both specific external input and input from intrastriatal FS interneurons. In fact, we expect that striatal FS interneuron input may be diminished in Parkinson's disease and in our experiments with carbachol, because ACh attenuates FS inhibition of MSNs through presynaptic muscarinic receptors (33). Thus, adding FS interneurons to the model will only affect the results of the normal, non-parkinsonian case. Because we are not trying to replicate all of the LFP patterns of the normal striatum but rather, explain the parkinsonian beta oscillation, we feel that a more complex model of the striatum with FS cells is not necessary. Similarly, we expect glutamatergic input from cortex and thalamus to be reduced, because activation of striatal M1 muscarinic receptors decreases both the probability of glutamate release from presynaptic terminals as well as the potency

of individual glutamatergic synapses onto MSNs (34). However, we expect striatal levels of ACh, which are thought to come mainly from striatal cholinergic interneurons, to be elevated in Parkinson's disease (15, 16). We note that anticholinergics were the only available pharmacologic treatment for Parkinson's disease until the introduction of L-dopa in the 1960s (35). Our model predicts that some of their efficacy may reside in their ability to decrease striatal beta oscillations.

The experimental results show additional changes not predicted by the computational models. The model does not predict the lower delta and theta frequency rhythms seen in the absence of carbachol. This may be due to the presence of other striatal cell types such as FS neurons not present in our model. Tremor-like activity is not a prediction of our model; beta oscillations in Parkinson's disease do not necessarily correlate with tremor (2). Even in the present study, however, the tremor can be viewed as interrupting the beta oscillation. The mouse beta oscillations are interrupted by periods of decreased beta before and after the tremor movement. We attribute this to some in vivo compensatory change in the response to increased beta in the striatum, possibly modulated by thalamic input, as there is evidence that parkinsonian tremor is modulated by the thalamus (36). Also, in the mice, there is a drifting in the frequency of beta, which attains its highest values postmovement, drifts to lower values, and disappears before the tremor movement. Our model provides several potential explanations for frequency drift, including changes to the GABAa or M-current conductances or changes in the background excitation. However, it is unclear which of these mechanisms might be contributing to the frequency drift in the mouse striatum. We also cannot account for the decreases in beta seen before the carbachol-induced rise in beta, which might represent a homeostatic response to the carbachol infusion. However, the decrease in beta that follows the rise in beta may be due to overrecovery of the M-current, in which increases in the M-current follow its suppression (37). Differences between our study and other published studies as well as other models of striatal MSNs are discussed in *SI Note 9*: *Other Related Studies*.

Other studies suggest that the enhanced beta rhythms in Parkinson's disease may arise from the interaction of the STN and the GPe or from the cortical patterning of STN (3). Both theories were developed initially from experimental studies showing very low frequency oscillations (less than 1.8 Hz) developing in structures relevant to Parkinson's disease (4, 5). In contrast, our studies on striatum show the emergence of robust beta frequency oscillations in both our computational and experimental results. Computational models of the STN-GPe network show that, under certain conditions, the system exhibits rhythmic oscillations within the frequency range appropriate to Parkinson's disease (3, 38). Interestingly, the critical condition for this to occur is increased inhibitory input from the striatum; increased patterned inhibitory input is a prediction of our model. Furthermore, the failure of cortical infusions of carbachol to induce beta oscillations is evidence against the idea that increasing gain anywhere within the cortico-basal ganglia-thalamic loop is sufficient to produce beta oscillations. Additionally, most of the mechanisms of beta production that we are currently aware of in the cortex are completely different from the mechanism of beta rhythm generation that we describe in our striatal model, and depend on excitatory cells (39, 40). One study using rat brain slices shows that high beta can be elicited from M1 by coapplication of carbachol and kinate (6). This beta rhythm appears to be dependent on networks of GABAergic interneurons as well as on excitatory cell drive similar to our model of striatum. However, Yamawaki et al. (6) think the mechanism of beta in M1 is similar to the mechanism producing persistent gamma oscillations in other cortical areas.

The results presented here highlight the powerful combination of mathematical and experimental approaches in addressing problems in systems neuroscience. Dynamics of biological systems do not readily yield to direct observation using even the most sophisticated experimental approaches. We show here that informed biophysical modeling can be highly predictive of complex biological dynamics. Additionally, these findings also have broad implications in understanding beta oscillations in normal motor function as well as their inappropriate expression in other disorders with striatal involvement.

Computational Methods

MSNs. We model MSNs using single-compartment models with Hodgkin–Huxley-type dynamics. Membrane currents (I_{memb}) consist of a fast sodium current (I_{na}), a fast potassium current (I_k), a leak current (I_L), and an M-current (I_m) (12). We do not model MSN up and down states, which are prevalent during sleep and anesthesia, because these transitions are not prevalent in the awake state (41), which is the focus of our model. Therefore, in our model MSNs, we do not include Kir2 currents, which are active in the MSN down state. The sum of all excitatory input from the cortex and thalamus is modeled using a background excitation term (I_{app}) and Gaussian noise.

Networks. MSNs connect primarily to other MSNs through GABAergic synapses (42). The GABAa current (I_{GABAa}) is modeled using a Hodgkin–Huxley-type conductance with weak GABAa maximal conductances.

MSNs have extensive local axonal projections that mainly contact other MSNs (42). We construct a striatal model with 100 MSNs and examine several patterns of network connectivity: all-to-all connections, nearest neighbor connections, and 30% random connections, which approximates the rate of connectivity found in both slice and cortex-striatum-substantia nigra organotypic cultures (32, 43).

Parkinsonian Striatum. We model the effect of loss of dopamine indirectly through its effect on ACh-induced reduction of the M-current. Thus, we model the parkinsonian striatum by reducing the maximal M-current conductance from 1.3 to 1.2 mS/cm^2.

LFP. MSNs account for 90–95% of all neurons in the rat neostriatum (44). LFPs are modeled as the sum of all MSN to MSN GABAa currents.

Stationarity of the network appears in the raster plots after ~700 ms. To ensure stationarity, our LFP is evaluated only after 1,000 ms of simulated time.

More details are in *SI Computational Methods*.

Experimental Methods

All procedures were done in accordance with the National Institutes of Health Guide for Laboratory Animals and were approved by the Massachusetts Institute of Technology Animal Care and Use and Biosafety Committees. Adult C57 or Swiss Webster mice were used. Under isoflurane anesthesia, a custom-fabricated plastic head plate was surgically affixed to the skull. Adult mice were head-fixed and recorded awake with glass electrodes filled with saline. LFP was collected with a Multiclamp 700B amplifier, digitized with a Digidata 1440 and acquired with pClamp 10 software at a sampling rate of 20 kHz (Molecular Devices). Recordings and infusions in the striatum were made at the stereotactic coordinate (–0.2 to 0.8, 2.0–2.5, 3.0–3.5) that receives projections from both the motor and sensory cortices (45). Infusion in the cortex directly above the striatal infusion sites were at the stereotactic coordinate (–0.2 to 0.8, 2.0–2.5, 1.2–1.7). Carbamoylcholine chloride (Carbachol; from Sigma) was dissolved in saline and infused at a 0.2 μL/min rate. The infusion cannula was positioned ~300–700 μm away from the recording electrode tip.

The LFP power spectrum was obtained with Hilbert transform in Matlab. More details are in *SI Experimental Methods*.

ACKNOWLEDGMENTS. M.M. and N.K. acknowledge support from National Science Foundation Grant DMS-0717670. E.S.B. acknowledges funding from National Institutes of Health Director's New Innovator Award DP2 OD002002-01. X.H. acknowledges support from the Helen Hay Whitney Foundation Fellowship and National Institutes of Health Grant K99MH085944. N.K. acknowledges support from National Institutes of Health/National Institute of Neurological Disorders and Stroke Grant 1 R01 NS062955-01.

1. DeLong Mahlon R, Juncos Jorge L Parkinson's disease and other extrapyramidal movement disorders. *Harrison's Principles of Internal Medicine* (2008), eds Fauci AS, et al. Available at http://www.accessmedicine.com/content.aspx?aID=2905868.
2. Brown P (2007) Abnormal oscillatory synchronisation in the motor system leads to impaired movement. *Curr Opin Neurobiol* 17:656–664.
3. Bevan MD, Magill PJ, Terman D, Bolam JP, Wilson CJ (2002) Move to the rhythm: Oscillations in the subthalamic nucleus-external globus pallidus network. *Trends Neurosci* 25:525–531.
4. Plenz D, Kital ST (1999) A basal ganglia pacemaker formed by the subthalamic nucleus and external globus pallidus. *Nature* 400:677–682.
5. Magill PJ, Bolam JP, Bevan MD (2001) Dopamine regulates the impact of the cerebral cortex on the subthalamic nucleus-globus pallidus network. *Neuroscience* 106: 313–330.
6. Yamawaki N, Stanford IM, Hall SD, Woodhall GL (2008) Pharmacologically induced and stimulus evoked rhythmic neuronal oscillatory activity in the primary motor cortex in vitro. *Neuroscience* 151:386–395.
7. Wichmann T, Smith Y, Vitek JL (2002) Pathophysiology of Parkinson's Disease in Chapter 22: Basal ganglia anatomy and physiology. *Parkinson's Disease: Diagnosis and Clinical Management* (online version), eds Factor SA, Weiner WJ (Demos Medical Publishing, New York).
8. Tepper JM, Bolam JP (2004) Functional diversity and specificity of neostriatal interneurons. *Curr Opin Neurobiol* 14:685–692.
9. Kish LJ, Palmer MR, Gerhardt GA (1999) Multiple single-unit recordings in the striatum of freely moving animals: Effects of apomorphine and D-amphetamine in normal and unilateral 6-hydroxydopamine-lesioned rats. *Brain Res* 833:58–70.
10. McCarthy MM, Brown EN, Kopell N (2008) Potential network mechanisms mediating electroencephalographic beta rhythm changes during propofol-induced paradoxical excitation. *J Neurosci* 28:13488–13504.
11. Pervouchine DD, et al. (2006) Low-dimensional maps encoding dynamics in entorhinal cortex and hippocampus. *Neural Comput* 18:2617–2650.
12. Shen W, Hamilton SE, Nathanson NM, Surmeier DJ (2005) Cholinergic suppression of KCNQ channel currents enhances excitability of striatal medium spiny neurons. *J Neurosci* 25:7449–7458.
13. Kreitzer AC (2009) Physiology and pharmacology of striatal neurons. *Annu Rev Neurosci* 32:127–147.
14. Costa RM, et al. (2006) Rapid alterations in corticostriatal ensemble coordination during acute dopamine-dependent motor dysfunction. *Neuron* 52:359–369.
15. DeBoer P, Heeringa MJ, Abercrombie ED (1996) Spontaneous release of acetylcholine in striatum is preferentially regulated by inhibitory dopamine D_2 receptors. *Eur J Pharmacol* 317:257–262.
16. Ikarashi Y, Takahashi A, Ishimaru H, Arai T, Maruyama Y (1997) Regulation of dopamine D_1 and D_2 receptors on striatal acetylcholine release in rats. *Brain Res Bull* 43:107–115.
17. Tseng KY, Kasanetz F, Kargieman L, Riquelme LA, Murer MG (2001) Cortical slow oscillatory activity is reflected in the membrane potential and spike trains of striatal neurons in rats with chronic nigrostriatal lesions. *J Neurosci* 21:6430–6439.
18. Chang JY, Shi LH, Luo F, Woodward DJ (2006) Neural responses in multiple basal ganglia regions following unilateral dopamine depletion in behaving rats performing a treadmill locomotion task. *Exp Brain Res* 172:193–207.
19. Brown P, Williams D (2005) Basal ganglia local field potential activity: Character and functional significance in the human. *Clin Neurophysiol* 116:2510–2519.
20. Mallet N, et al. (2008) Parkinsonian beta oscillations in the external globus pallidus and their relationship with subthalamic nucleus activity. *J Neurosci* 28:14245–14258.
21. Devos D, et al. (2006) Predominance of the contralateral movement-related activity in the subthalamo-cortical loop. *Clin Neurophysiol* 117:2315–2327.
22. Pfurtscheller G, Stancák A, Jr., Neuper C (1996) Post-movement beta synchronization. A correlate of an idling motor area? *Electroencephalogr Clin Neurophysiol* 98:281–293.
23. Sochurkova D, Rektor I (2003) Event-related desynchronization/synchronization in the putamen. An SEEG case study. *Exp Brain Res* 149:401–404.
24. Koos T, Tepper JM, Wilson CJ (2004) Comparison of IPSCs evoked by spiny and fast-spiking neurons in the neostriatum. *J Neurosci* 24:7916–7922.
25. Bracci E, Panzeri S (2006) Excitatory GABAergic effects in striatal projection neurons. *J Neurophysiol* 95:1285–1290.
26. Tunstall MJ, Oorschot DE, Kean A, Wickens JR (2001) Inhibitory interaction between spiny projection neurons in the rat striatum. *J Neurophysiol* 88:1263–1269.
27. Liang L, DeLong MR, Papa SM (2008) Inversion of dopamine responses in striatal medium spiny neurons and involuntary movements. *J Neurosci* 28:7537–7547.
28. Hardman CD, et al. (2002) Comparison of the basal ganglia in rats, marmosets, macaques, baboons, and humans: Volume and neuronal number for the output, internal relay, and striatal modulating nuclei. *J Comp Neurol* 445:238–255.
29. Stanford IM (2003) Independent neuronal oscillators of the rat globus pallidus. *J Neurophysiol* 89:1713–1717.
30. Chan CS, Shigemoto R, Mercer JN, Surmeier DJ (2004) HCN2 and HCN1 channels govern the regularity of autonomous pacemaking and synaptic resetting in globus pallidus neurons. *J Neurosci* 24:9921–9932.
31. Albin RL, Young AB, Penney JB (1989) The functional anatomy of basal ganglia disorders. *Trends Neurosci* 12:366–375.
32. Taverna S, Ilijic E, Surmeier DJ (2008) Recurrent collateral connections of striatal medium spiny neurons are disrupted in models of Parkinson's disease. *J Neurosci* 28: 5504–5512.
33. Koós T, Tepper JM (2002) Dual cholinergic control of fast-spiking interneurons in the neostriatum. *J Neurosci* 22:529–535.
34. Higley MJ, Soler-Llavina GJ, Sabatini BL (2009) Cholinergic modulation of multivesicular release regulates striatal synaptic potency and integration. *Nat Neurosci* 12:1121–1128.
35. Pisani A, Bernardi G, Ding J, Surmeier DJ (2007) Re-emergence of striatal cholinergic interneurons in movement disorders. *Trends Neurosci* 30:545–553.
36. Putzke JD, et al. (2003) Thalamic deep brain stimulation for tremor-predominant Parkinson's disease. *parkinsonism Relat Disord* 10:81–88.
37. Pfaffinger P (1988) Muscarine and t-LHRH suppress M-current by activating an IAP-insensitive G-protein. *J Neurosci* 8:3343–3353.
38. Terman D, Rubin JE, Yew AC, Wilson CJ (2002) Activity patterns in a model for the subthalamopallidal network of the basal ganglia. *J Neurosci* 22:2963–2976.
39. Roopun AK, et al. (2008) Period concatenation underlies interactions between gamma and beta rhythms in neocortex. *Front Cell Neurosci*, 10.3389/neuro. 03.001.2008.
40. Roopun AK, et al. (2010) Cholinergic neuromodulation controls directed temporal communication in neocortex in vitro. *Front Neural Circuits* 4:8.
41. Mahon S, et al. (2006) Distinct patterns of striatal medium spiny neuron activity during the natural sleep-wake cycle. *J Neurosci* 26:12587–12595.
42. Tepper JM, Wilson CJ, Koós T (2008) Feedforward and feedback inhibition in neostriatal GABAergic spiny neurons. *Brain Res Brain Res Rev* 58:272–281.
43. Czubayko U, Plenz D (2002) Fast synaptic transmission between striatal spiny projection neurons. *Proc Natl Acad Sci USA* 99:15764–15769.
44. Koós T, Tepper JM (1999) Inhibitory control of neostriatal projection neurons by GABAergic interneurons. *Nat Neurosci* 2:467–472.
45. Ramanathan S, Hanley JJ, Deniau JM, Bolam JP (2002) Synaptic convergence of motor and somatosensory cortical afferents onto GABAergic interneurons in the rat striatum. *J Neurosci* 22:8158–8169.

Supporting Information

McCarthy et al. 10.1073/pnas.1107748108

SI Note 1: M-Current in Model Produces Rhythms With or Without GABAa Connections

The M-current enables our medium spiny neurons (MSNs) to spike as a population at around 8 Hz independent of GABAa connections. Specifically, MSNs with an M-current respond to Gaussian noise with a subthreshold voltage oscillation around 8 Hz. Thus, an individual MSN is most likely to spike at the peak of one of the 8-Hz subthreshold membrane oscillations, which is evidenced by the increased number of MSN interspike intervals between 111 and 200 ms when MSNs are allowed to spike independently of each other (Fig. S2*B*). The 8-Hz oscillation in the local field potential (LFP) is not because of network synchronization, because there is no network coupling; rather, because MSNs tend to spike several times in row at 8 Hz due to the subthreshold oscillation, this frequency is being picked up in the LFP.

Two important things happen as we add GABAa connections to our model MSNs. First, the MSNs become more synchronized as expected upon the addition of synaptic connections. Second, the peak beta frequency increases. This increased frequency can be explained by the time constant of decay of the M-current, which has lower values for more hyperpolarized voltages. Thus, a small amount of GABAa conductance leads to a small hyperpolarization that pushes the time to rebound into what is appropriate for the low beta range. Larger amounts of GABAa conductance (as in the Parkinson's case because the MSNs are more synchronized) result in a faster time to rebound and a higher beta frequency peak. Because the spiking rate of individual MSNs stays low as GABAa connections are added under normal conditions ($\bar{g}_m$ = 1.3 mS/cm^2), intrinsic MSN properties likely set the normal spiking rate in the model. However, the strength of the GABAa connections modulates the network frequency.

Previous work (1) suggested that some range of GABAa conductances leads to an increase in beta power and peak beta frequency. A brief description of this mechanism can be found in *SI Note 5: Mechanism of M-current/GABAa current interaction involved in production of beta frequency oscillations between inhibitory neurons*. However, because the current network is different from the network in McCarthy et al. (1), we tested to see if changes in the GABAa conductance affect beta power. The power and frequency of the beta oscillation tend to change nonmonotonically as the GABAa conductance is increased (Fig. S3*A*). The peak frequency reaches a maximum of about 16.6 Hz when the GABAa conductance is at its maximal tested value of 1.0 mS/cm^2. The average spiking rate of the MSNs changes nonmonotonically as the GABAa conductance strength is increased (Fig. S3*B*). We note that, within this range of GABAa conductance strengths, the average MSN spiking rate remains between 0.9 and 1.82 Hz, within what we consider the normal range.

The lower limit of the beta oscillation frequency observed in Parkinson's disease is 8 Hz (2, 3). We are not looking at the oscillations that have been found in recordings from neurons in the globus pallidus (GP) and subthalamic nucleus (STN) that may be of lower frequency (<8 Hz) and may be more related to the parkinsonian tremor (4–6). In our models with MSN M-current present, we can think of the 8-Hz oscillation in a population of unconnected MSNs as the limiting frequency as GABAa conductance is lowered. Except for a small region around zero conductance, increasing the GABAa conductance strength both increases the peak frequency of the beta oscillation and patterns the population of MSNs into a more obvious beta frequency rhythm.

SI Note 2: Changes in M-Current Conductance and I_{app} Modulate the Peak Frequency and Power of the LFP Beta Oscillation

The maximal M-current conductance modulates the peak frequency of the beta oscillation. Both the power and peak of the beta frequency oscillation decrease as the M-current conductance increases over the range from 1.1 to 1.4 mS/cm^2 (Fig. S3*C*). The peak beta frequency is maximal around 21 Hz when the M-current is at its lowest tested value of 1.1 mS/cm^2. The peak beta frequency is about 11 Hz when the M-current conductance is 1.3 mS/cm^2. Very small additional increases in the M-current conductance result in a loss of the beta oscillation. Also, the spiking rate of the MSNs decreases with increases in M-current conductance (Fig. S3*D*).

Increasing the background excitation (I_{app}) increases both the frequency and power of the peak beta oscillation (Fig. S3*E*) as well as the average spiking rate of the MSNs (Fig. S3*F*). At the highest value of I_{app} tested, the beta frequency oscillation peaks at about 22 Hz. At lower values of I_{app} ranging from about 1.19 to 1.23 μA/cm^2, the beta oscillation peaks between ∼9 and 14 Hz. At the lowest values of I_{app}, the beta oscillation disappears.

SI Note 3: Network Model of Fast-Spiking Interneurons Can Also Produce 8- To 30-Hz Oscillations But Not in the Physiologic Range

Striatal fast-spiking (FS) interneurons are electrically connected (7), suggesting that coordinated activity of FS interneurons is possible. Furthermore, FS interneurons predominately target MSNs (8) and provide much stronger inhibition to MSNs than is provided by MSN to MSN connections (9). Moreover, estimates suggest that a single FS interneuron can interact with ∼135 MSNs (8). These properties of striatal FS interneurons potentially provide a means of synchronizing a large population of MSNs. Thus, we model FS interneurons to examine whether their network interactions can account for our experimental observations.

FS interneurons are modeled in the same way as MSNs except that they lack an M-current and have electrical connections (7). We add electrical connections between an FS interneuron and its two nearest neighbors. The current from an electrical synapse is modeled as (Eq. **S1**)

$$I_e = g_e\left(V_{post} - V_{pre}\right). \qquad \textbf{[S1]}$$

The maximal conductance of the electrical synapses (g_e) is set at 0.01 mS/cm^2. Because carbachol (0.1 mM) excites and increases the spiking frequency of FS interneurons in vitro (10), we model the addition of carbachol by increasing the background excitation (I_{app}) to the model.

We find that, for FS interneuron spiking rates between 0.45 and 12.1 Hz, a population oscillation between ∼8 and 30 Hz emerges in our network models (I_{app} = 0.12–0.38 μA/cm^2). We show that, in a population consisting entirely of FS interneurons, 8- to 30-Hz rhythms are both possible and modulated by background excitation (Fig. S4). Similar to our model with MSNs, this model shows that, as the background excitation is increased within a certain range, the peak frequency of the population oscillation increases (Fig. S4*E*). We also observed increases in spiking rate as the background excitation is increased.

We consider this model less accurate than the MSN model. FS interneurons have an average spiking rate of 24.7 Hz in vivo in awake rats (11). Giving our model FS interneurons, an average spiking rate of ∼24 Hz leads to clusters of interneurons spiking

fairly antisynchronously with a population frequency around 50 Hz. The model LFP power has several peaks, the highest of which is around 100 Hz followed by 50-, 75-, 1.5-, and 25-Hz peaks. This was not observed in our experimental mouse data before carbachol infusion. Furthermore, because carbachol (0.1 mM) increases FS interneuron excitation and spiking frequency in vitro, our FS model predicts that we may see increased gamma frequency (30–100 Hz) peaks in the power spectrum after carbachol infusion. However, prominent gamma frequency peaks were not observed in the mouse striatum either before or after carbachol infusion (0.1–0.2 mM). For these reasons, the mechanism shown in the FS interneuron network model may not be relevant to beta rhythm production in striatum.

SI Note 4: Model Results are Largely Invariant to Changes in Network Connectivity, Network Size, and Heterogeneity

Striatal networks with either nearest neighbor or random network connections give qualitatively similar results to the network with all-to-all connections. In each case, the average MSN spiking rate is between 0.5 and 2 Hz in the normal, non-parkinsonian states. In all three network topologies, the model LFPs show a distinct peak in the beta frequency range (Fig. S5*A*). Furthermore, in each type of network, the peak LFP power in the parkinsonian state both increases and shifts to a higher beta frequency than in the non-parkinsonian cases, and the average MSN spiking rate increases above normal.

Increasing the number of MSNs to 400 gives qualitatively similar results to our model with 100 neurons under the most destabilizing of conditions tested (random network connections of 30% and 7.5% connectivity) (Fig. S5*B*). In both cases, distinct peaks in the beta frequency range emerge. The beta peak under parkinsonian conditions is both larger in power and shifted to a higher beta frequency, which is also seen in the model using 100 neurons.

Introducing heterogeneity by giving individual MSNs different maximal GABAa conductances leads to qualitatively similar behavior to the network in which all maximal GABAa conductances are the same for each MSN (Fig. S6), with the exception of some temporary suppression of MSNs that are receiving larger GABAa conductance in the parkinsonian state. However, this temporary suppression of MSNs does not disrupt the increased LFP beta power in the parkinsonian state. Furthermore, heterogeneity helps us distinguish between the models of MSNs with and without M-current. MSNs without M-current are not robust to heterogeneity, and the low beta peak shows only a minor rise after increasing excitation to simulate the addition of carbachol (peak LFP beta power rises 2.6 dB between normal and parkinsonian conditions when MSNs lack M-current vs. a 7.42 dB rise when MSNs have M-currents). MSN networks in vivo likely contain significant heterogeneity in GABAa conductances (9). Therefore, the model with M-current present in the MSNs is the more plausible model. Previous work shows that the GABAa/M-current interaction can mediate the time to rebound spiking (1), a major determinant in setting the frequency of oscillatory activity within a network, suggesting that the M-current/GABAa interaction is a major determinant of the oscillatory frequency within our network of MSNs with M-current present.

SI Note 5: Mechanism of M-Current/GABAa Current Interaction Involved in Production of Beta Frequency Oscillations Between Inhibitory Neurons

Here, we look at the interaction of single-compartment conductance-based model neurons with Hodgkin–Huxley dynamics. Each neuron contains the spiking currents (fast sodium, fast potassium, and leak) and an M-current. In a simple two-neuron system in which one neuron is connected unidirectionally to the other neuron by a GABAa synapse, rebound spiking can follow GABAa inhibition. If the neuron receiving GABAa input does not have the M-current, rebound spiking does not occur. Rebound spiking occurs, because the GABAa current temporarily brings the membrane potential closer to the reversal potential of potassium, thus reducing the M-current (Fig. S7*A*). Increasing the GABAa conductance causes the M-current to decrease further (Fig. S7*A*). Note that the M-current is not completely suppressed, because the reversal potential of the GABAa current (−80 mV) is higher than the reversal potential for potassium (−100 mV). Because the M-current is a potassium current, reduction of this current leads to greater membrane excitability, which enables the neuron to rebound spike. Two such neurons reciprocally connected form a stable rhythm in the beta frequency range (Fig. S7*B*).

The time to rebound spiking after inhibition depends nonlinearly on both the amount of M-current and the amount of GABAa inhibition (Fig. S7*C*). We note that a wide range of M-current conductances allows for the time to rebound spiking to fall within the beta frequency range. Furthermore, if a resting neuron is induced to spike, either by transient excitation or rebound inhibition, then additional rebound spiking depends on both the timing of GABAa inhibition after the spike and the amount of GABAa inhibition (Fig. S7*D*). If GABAa inhibition is weak, as is the situation between MSNs, and the inhibition comes during the neuron's repolarization phase, then rebound spiking does not occur. Because the membrane potential is already close to the GABAa reversal potential during the repolarization phase, weak GABAa input will not alter the membrane potential much from its normal repolarization potentials, and the neuron will return to quiescence. However, potentiating GABAa allows GABAergic inhibition to last longer and induce rebound spiking even if the inhibition occurs during the repolarization phase. Thus, GABAa potentiation allows greater excitation of individual neurons and more participation of individual neurons in networks. Therefore, we expect potentiation of the maximal GABAa conductance to be able to increase participation of individual neurons in the network dynamics producing the beta frequency rhythm.

SI Note 6: Noise

Our modeling of MSNs derives from modeling work by McCarthy et al. (1). However, in that study, the interneurons do not have noise (1). It is unclear from this previous study if a noisy system with low individual neuronal spiking rates and weak GABAa synapses is capable of generating a population beta rhythm. The present study shows that a robust population beta frequency rhythm forms under these conditions. Noise allows the spiking rate of individual MSNs to be low. Even with very weak GABAa synapses between MSN neurons, the population of neurons is still able to maintain a robust beta frequency population oscillation. The beta frequency becomes more pronounced as the spiking rate of the MSNs increases, because additional MSN spiking increases the overall GABAa current received by each neuron. This, in turn, increases the probability for MSN rebound spiking and patterning of the MSNs into the ongoing population beta rhythm (related work by Brunel and Hakim) (12).

SI Note 7: Reversal Potentials

Several experiments have suggested different GABAa reversal potentials in the MSNs of the striatum (9, 13, 14). The experiment showing the lowest GABAa reversal potential comes from two perforated patch recordings. The experimental animal was the Sprague–Dawley rat, and at least one recording was from a 13-d-old rat. The experiment showing a reversal potential of −62 mV comes from slice studies with Wister rats, which were 24–28 d old (n = 5). The experiment showing a reversal potential of −64 mV comes from slice studies with Wister rats, which were 18–28 d old. The differences in the experiments could be accounted for by the different breeds of rats, the differences in ages, or the different number of rats used in each experiment.

SI Note 8: Other Currents in MSNs

Additional study of this system will reveal the extent to which modulators of GABAa and the M-current can create beta rhythms in the MSN network independent of both the effects of other striatal GABAergic interneurons and the influence of, potentially, the entire cortico-basal ganglia-thalamic loop. Acetylcholine (ACh) has several other actions on M1 muscarinic receptors (mAChRs), which suggest that activation of mAChRs will increase MSN excitability. These actions include inhibition of Kir-currents, a shift in the inactivation of A-type potassium currents to lower membrane potentials, and inhibition of N- and P/Q-type calcium channels, which affect calcium-activated potassium channels and cause increased MSN spiking (7). Thus, these additional currents may play a role in increasing MSN excitability, which as our results show may increase beta frequency rhythms in the MSN network. However, unlike the M-current, neither the A-type potassium current nor the non-inactivating Kir-current has the appropriate kinetics to generate beta rhythms by the mechanism that we describe here (15, 16).

SI Note 9: Other Related Studies

Orphenadrine. In contrast to our results, a previous study reports that the anticholinergic orphenadrine increased rather than decreased beta power in the STN (17). However, the dose of orphenadrine used did not improve bradykinesia, a symptom that has been correlated to beta frequency oscillations in Parkinson's disease (18). Furthermore, although orphenadrine is classified as an antimuscarinic agent, it has been shown to have low affinity for muscarinic receptors (19).

Phase Relationships. Several other studies indicate that the beta oscillations recorded over the cortical motor areas phase lead the beta activity in the STN and GP, suggesting that the cortical beta rhythms may be driving the beta rhythms in the STN and GP (20–22). However, this does not imply that the beta oscillations originate in the cortex, because oscillations originating in other places could give rise to such phase relationships.

Other Models. We also note that several other studies have used models of striatal MSNs to look at oscillatory behavior in striatum. A modeling study by Kitano et al. (23) uses a two-compartment model of MSNs to examine the influence of corticostriatal inputs on correlated subthreshold depolarized states. No MSN to MSN connections or any other GABAergic connections are present, which makes this study fundamentally different from ours.

A study by Wolf et al. (15) looked for entrainment of MSNs to oscillations in the theta range (4–12 Hz), which partially overlaps our beta range between 8 and 12 Hz. The modeling study consists of one MSN modeled with 169 compartments. AMPA, NMDA, and GABAa inputs to the MSN are put in by hand. Wolf et al. (15) find that the NMDA to AMPA ratio has a large influence on the ability of the MSN to entrain oscillatory glutamatergic input in the theta range. In contrast, our modeling study focuses on intrinsic striatal GABAergic input to MSNs from other MSNs and the ability of MSNs to interact with each other to create rhythms.

A study by Humphries et al. (24) examines the dynamics of a 3D model of striatal MSNs and FS interneurons interconnected by GABAergic synapses. They find that lack of dopamine produced the formation of clusters of synchronized MSNs. Our model also predicts increased synchronization of MSNs with loss of dopamine or increased levels of ACh. However, we also suggest that the synchronization has an oscillatory component in the beta frequency range. Furthermore, in the study by Humphries et al. (24), the MSNs are modeled using an extension of a model of neuron dynamics introduced by Izhikevich (25), and they lack explicit intrinsic membrane currents. In comparison, our model dynamics depend on the interaction of the intrinsic membrane M-current and the synaptic GABAa current.

SI Computational Methods

MSNs. MSNs account for 95% of striatal neurons (8). Our resting membrane potential is around −63.8 mV, which is near the peak of the distribution (−63.5 mV) of resting membrane potentials measured in the awake state in vivo (26). Setting I_{app} = 1.19 μA/cm^2 and the amplitude of the noise to $4\sqrt{\Delta t}$, where Δt is the time step of integration, gives the model MSNs enough background excitation for their resting membrane potential to be −63.8 mV (26) and their average baseline spiking rate to be ∼1 Hz (27). MSNs are synaptically interconnected by GABAa receptors. Each membrane current is modeled using Hodgkin–Huxley-type conductance dynamics, and each current has a constant maximal conductance and reversal potential taken from a previous model (1), except for the maximal conductance of the M-current ($\bar{g}_m$), which is set at 1.3 mS/cm^2 for the normal striatum and lowered, as described below, to simulate the parkinsonian striatum.

The voltage (V) change in each neuron is described by (Eq. S2)

$$c_m \frac{dV}{dt} = -\sum I_{memb} - \sum I_{syn} + I_{app}. \qquad \text{[S2]}$$

Specific membrane capacitance (c_m) is held constant at 1 μF/cm^2. In the absence of noise, a 6-Hz oscillation emerges as the level of background excitation (I_{app}) is increased because of a Hopf bifurcation, a well-known mechanism in nonlinear dynamics producing the sudden onset of nonzero frequency oscillations (28). A lower average spiking rate in the 0.5- to 2-Hz range can be obtained by adding Gaussian noise of mean zero and SD one (amplitude of the noise is $4\sqrt{\Delta t}$, where Δt is the time step of integration) to the background excitation term (I_{app} = 1.19 μA/cm^2). The noise gives voltage fluctuations of, at most, about 3 mV. We do not model the up and down states of the MSNs because these two resting membrane potential states are not prevalent in the awake state (26).

Each membrane current is modeled using Hodgkin–Huxley-type conductance dynamics formulated as (Eq. S3)

$$I = \bar{g}\left(m^n h^k\right)(V - E_{ion}). \qquad \text{[S3]}$$

Each current has a constant maximal conductance ($\bar{g}$) and reversal potential (E_{ion}). The activation (m) and inactivation (h) gating variables have n and k order kinetics, respectively, where $n, k \geq 0$. Each gating variable evolves in time according to a two-state kinetic equation formulated (written for the gating variable m) as (Eq. S4)

$$\frac{dm}{dt} = \frac{m_\infty - m}{\tau_m}. \qquad \text{[S4]}$$

The steady-state function (m_∞) and the time constant of decay (τ_m) are taken from a previous model (1) and relate to the rate functions for each current (α_m and β_m) by (Eqs. S5 and S6)

$$m_\infty = \alpha_m/(\alpha_m + \beta_m), \qquad \tau_m = 1/(\alpha_m + \beta_m). \qquad \text{[S5 and S6]}$$

The maximal sodium conductance is $\bar{g}_{Na} = 100 mS/cm^2$, and the sodium reversal potential is E_{Na} = 50 mV. The sodium current has three activation gates (n = 3) and one inactivation gate (k = 1). The rate functions for the sodium current activation (m) and inactivation (h) variables are described by (Eqs. S7–S10)

$$\alpha_m = \frac{0.32(V+54)}{1-\exp[-(V+54)/4]}, \quad \text{[S7]}$$

$$\beta_m = \frac{0.28(V+27)}{\exp[(V+27)/5]-1}, \quad \text{[S8]}$$

$$\alpha_h = 0.128\exp[-(V+50)/18], \quad \text{[S9]}$$

$$\beta_h = \frac{4}{1+\exp[-(V+27)/5]}. \quad \text{[S10]}$$

The maximal conductance for the fast potassium channel is $\bar{g}_K = 80\,mS/cm^2$, and the reversal potential for potassium is $E_K = -100$ mV. The fast potassium channel has no inactivation gates but has four activation gates described by the rate functions (Eqs. **S11** and **S12**)

$$\alpha_m = \frac{0.032(V+52)}{1-\exp[-(V+52)/5]}, \quad \text{[S11]}$$

$$\beta_m = 0.5\exp[-(V+57)/40]. \quad \text{[S12]}$$

The leak current (I_L) has no gating variables. The maximal leak channel conductance is ($\bar{g}_L$) = 0.1 mS/cm^2, and the leak channel reversal potential is $E_L = -67$ mV.

The M-current has one activation gate and no inactivation gate. The maximal conductance for the M-current, $\bar{g}_m$, is 1.3 mS/cm^2 when we simulate the normal striatum and 1.2 mS/cm^2 when we simulate the parkinsonian striatum. The rate functions for the M-current activation variable are given by (Eqs. **S13** and **S14**)

$$\alpha_m = \frac{Q_s 10^{-4}(V+30)}{1-\exp[-(V+30)/9]}, \quad \text{[S13]}$$

$$\beta_m = -\frac{Q_s 10^{-4}(V+30)}{1-\exp[(V+30)/9]}. \quad \text{[S14]}$$

For the M-current, a Q_{10} factor of 2.3 is used in scaling the rate functions, because the kinetics were originally derived from experiments performed at 23 °C. At a normal body temperature of 37 °C, the rate equations for the M-current are scaled by (Eq. **S15**)

$$Q_s = Q_{10}^{(37^\circ C - 23^\circ C)/10} = 3.209. \quad \text{[S15]}$$

Networks. MSNs interact with other MSNs through relatively weak GABAa synaptic conductances (8, 9). The GABAa current (I_{GABAa}) is modeled using a Hodgkin–Huxley-type conductance (Eq. **S16**):

$$I_{GABAa} = \frac{\bar{g}_{ii}}{N} s_i (V - E_i). \quad \text{[S16]}$$

The GABAa connections between MSNs are weak and mostly located on the dendrites (8, 9). Thus, we use very weak GABAa conductances in our model neurons. The maximal conductance of the GABAa current ($\bar{g}_{ii}/N$) is set to $0.1/N$ mS/cm^2, where N is the number of synaptic connections made onto the neuron. Thus, the maximal GABAa conductance from one MSN to another MSN is 0.001 mS/cm^2 in an all-to-all connected network and 0.003 mS/cm^2 in our two 30% connected networks.

The variable s_i represents the gating variable for inhibitory GABAa synaptic transmission. For the jth MSN in the system (Eq. **S17**),

$$s_i = \sum_{k=1}^{N} S_{i_k i_j}. \quad \text{[S17]}$$

The synaptic kinetics of the gating variable from the kth MSN to the jth MSN ($S_{i_k i_j}$) evolves according to the first-order differential equation (Eq. **S18**)

$$\frac{dS_{i_k i_j}}{dt} = g_{GABAa}(V_k)(1 - S_{i_k i_j}) - \frac{S_{i_k i_j}}{\tau_i}. \quad \text{[S18]}$$

We use a GABAa time constant (τ_i) of 13 ms to match experimental results (29). The reversal potential of the GABAa current (E_i) is set to −80 mV. The rate function for the open state of the GABAa receptor, $g_{GABAa}(V_k)$ is formulated as (Eq. **S19**)

$$g_{GABAa}(V_k) = 2\left(1 + tanh\left(\frac{V_k}{4}\right)\right). \quad \text{[S19]}$$

For randomly connected networks, we simulate several trials and average the results. Heterogeneity is given to some networks by letting the maximal GABAa conductance to each MSN vary uniformly between 0.1 and 0.6 mS/cm^2.

MSNs have extensive local axonal projections that mainly contact other MSNs (8). We construct a striatal model with 100 MSNs and examine several patterns of network connectivity. All-to-all networks consist of each MSN in the network connected to all other MSNs. Autapses are not allowed. Nearest neighbor connections are simulated by allowing each MSN to connect to its 30 nearest neighbors; therefore, if we line up the 100 MSNs on the circumference of a circle, each MSN connects to the closest 15 MSNs on its right and the closest 15 MSNs on its left. Random network connections are simulated by allowing each MSN to connect randomly to 30 other MSNs. This approximates the rate of connectivity found in both slice and cortex-striatum-substantia nigra organotypic cultures (29, 30). Reciprocal connections are allowed, because reciprocal connections between MSNs occur at the rate assumed by random connectivity in organotypic cultures (30). The mean percentage of reciprocally connected pairs of MSNs is 31% (maximum = 32% and minimum = 29%). For the randomly connected network with 100 neurons, we simulate 10 trials of such networks with different random connections and average the results. For the randomly connected network with 400 neurons (here we use both 30% and 7.5% random connectivity), we simulate three trials of 3 s each and average the results.

LFP. MSNs account for 90–95% of all neurons in the rat neostriatum (31), whereas the larger cholinergic neurons account for only 0.3% of the striatal neurons (10). Therefore, most of the current flow contributing to the generation of the striatal LFP is most likely attributable to the flow within the MSNs. LFPs are modeled as the sum of all GABAa currents, because LFP potentials are commonly thought to be the result of synaptic activity on the dendrites (32). MSN to MSN connections are located on the dendrites. We use inhibitory post-synaptic currents (IPSCs) because the fast locally generated currents in striatum are all inhibitory. We use locally generated currents, because we are interested in how the striatum itself can generate the beta rhythms as opposed to responding to rhythms imposed by external inputs. Experimental work shows that at least some portion of the rat neostriatal LFP signal correlates with neuronal hyperpolarization and inhibition of neuronal spiking (33), suggesting that the LFP is reflecting the effect of local GABAergic currents. Furthermore, a portion of the rat neostriatal LFP was also found to be caused by neuronal spiking (33). The GABAa currents in our model reflect the spiking activity of MSNs. Synaptic currents have been used in other models of the LFP, the

electroencephalogram (EEG) and the magnetoencephalogram (MEG). (1, 34, 35).

In simulations in which the neurons were unconnected and thus, lacked GABAa currents, we approximated the LFP by using the sum of all of the GABAa conductances that would have been present if GABAa connections had been present. Thus, the approximation of the LFP in this case reflected neuronal spiking. We use the multitaper method for calculating the power spectral density (36). We use seven discrete prolate spheroidal sequences for data tapers.

Statistics. Models were run 10 times over 5 simulated seconds. The mean and SD were calculated for the MSN average spiking rates and the peak frequency for the model LFP oscillations from these trials.

Computational Tools. Our network models were programmed in C++ and compiled using g++. The differential equations were integrated using a fourth-order Runge Kutta algorithm. The integration time step was 0.05 ms. Model output was graphed and analyzed using MatLab-R2009b.

SI Experimental Methods

The LFP power spectrum was obtained with the Hilbert transform in Matlab. Median beta power at 5-s intervals was first calculated for the entire time course of each experiment. Baseline beta power was calculated as the median during the 300 s before carbachol infusion started. Changes in beta power were determined using a *t* test comparing the median beta power of the 5-s period with the baseline median beta power. Because changes in beta power induced by drug infusion should be long-lasting, we considered a significant beta power change as any period when the beta power was higher or lower from the baseline for at least 30 s during any 40-s interval. The peak beta power (Fig. 2*F*) was determined as the peak increase in the median beta power of a 5-s interval. The beta power during the recovery period was calculated as the median value during the last 300 s of the experiment, typically 1,500–2,500 s after carbachol infusion had stopped. For control experiments, where no significant increase in beta power was observed (Fig. 2 *G–I*), the beta power upon carbachol infusion was calculated as the median during the 300-s period starting 450 s after infusion started, because the latency for beta power increase upon striatal carbachol infusion is 450 s.

1. McCarthy MM, Brown EN, Kopell N (2008) Potential network mechanisms mediating electroencephalographic beta rhythm changes during propofol-induced paradoxical excitation. *J Neurosci* 28:13488–13504.
2. Brown P, et al. (2001) Dopamine dependency of oscillations between subthalamic nucleus and pallidum in Parkinson's disease. *J Neurosci* 21:1033–1038.
3. Brown P, Williams D (2005) Basal ganglia local field potential activity: Character and functional significance in the human. *Clin Neurophysiol* 116:2510–2519.
4. Bergman H, Wichmann T, Karmon B, DeLong MR (1994) The primate subthalamic nucleus. II. Neuronal activity in the MPTP model of parkinsonism. *J Neurophysiol* 72: 507–520.
5. Nini A, Feingold A, Slovin H, Bergman H (1995) Neurons in the globus pallidus do not show correlated activity in the normal monkey, but phase-locked oscillations appear in the MPTP model of parkinsonism. *J Neurophysiol* 74:1800–1805.
6. Raz A, Vaadia E, Bergman H (2000) Firing patterns and correlations of spontaneous discharge of pallidal neurons in the normal and the tremulous 1-methyl-4-phenyl-1,2,3,6-tetrahydropyridine vervet model of parkinsonism. *J Neurosci* 20:8559–8571.
7. Kreitzer AC (2009) Physiology and pharmacology of striatal neurons. *Annu Rev Neurosci* 32:127–147.
8. Tepper JM, Wilson CJ, Koós T (2008) Feedforward and feedback inhibition in neostriatal GABAergic spiny neurons. *Brain Res Brain Res Rev* 58:272–281.
9. Koos T, Tepper JM, Wilson CJ (2004) Comparison of IPSCs evoked by spiny and fast-spiking neurons in the neostriatum. *J Neurosci* 24:7916–7922.
10. Tepper JM, Bolam JP (2004) Functional diversity and specificity of neostriatal interneurons. *Curr Opin Neurobiol* 14:685–692.
11. Berke JD (2008) Uncoordinated firing rate changes of striatal fast-spiking interneurons during behavioral task performance. *J Neurosci* 28:10075–10080.
12. Brunel N, Hakim V (1999) Fast global oscillations in networks of integrate-and-fire neurons with low firing rates. *Neural Comput* 11:1621–1671.
13. Bracci E, Panzeri S (2006) Excitatory GABAergic effects in striatal projection neurons. *J Neurophysiol* 95:1285–1290.
14. Tunstall MJ, Oorschot DE, Kean A, Wickens JR (2001) Inhibitory interaction between spiny projection neurons in the rat striatum. *J Neurophysiol* 88:1263–1269.
15. Wolf JA, et al. (2005) NMDA/AMPA ratio impacts state transitions and entrainment to oscillations in a computational model of the nucleus accumbens medium spiny projection neuron. *J Neurosci* 25:9080–9095.
16. Steephen JE, Manchanda R (2009) Differences in biophysical properties of nucleus accumbens medium spiny neurons emerging from inactivation of inward rectifying potassium currents. *J Comput Neurosci* 27:453–470.
17. Priori A, et al. (2004) Rhythm-specific pharmacological modulation of subthalamic activity in Parkinson's disease. *Exp Neurol* 189:369–379.
18. Kühn AA, Kupsch A, Schneider GH, Brown P (2006) Reduction in subthalamic 8-35 Hz oscillatory activity correlates with clinical improvement in Parkinson's disease. *Eur J Neurosci* 23:1956–1960.
19. Syvälahti EK, Kunelius R, Laurén L (1988) Effects of antiparkinsonian drugs on muscarinic receptor binding in rat brain, heart and lung. *Pharmacol Toxicol* 62:90–94.
20. Brown P (2003) Oscillatory nature of human basal ganglia activity: Relationship to the pathophysiology of Parkinson's disease. *Mov Disord* 18:357–363.
21. Fogelson N, et al. (2006) Different functional loops between cerebral cortex and the subthalmic area in Parkinson's disease. *Cereb Cortex* 16:64–75.
22. Williams D, et al. (2002) Dopamine-dependent changes in the functional connectivity between basal ganglia and cerebral cortex in humans. *Brain* 125:1558–1569.
23. Kitano K, Aoyagi T, Fukai T (2001) A possible functional organization of the corticostriatal input within the weakly-correlated striatal activity: A modeling study. *Neurosci Res* 40:87–96.
24. Humphries MD, Wood R, Gurney K (2009) Dopamine-modulated dynamic cell assemblies generated by the GABAergic striatal microcircuit. *Neural Netw* 22:1174–1188.
25. Izhikevich EM (2007) *Dynamical Systems in Neuroscience* (MIT Press, Cambridge, MA).
26. Mahon S, et al. (2006) Distinct patterns of striatal medium spiny neuron activity during the natural sleep-wake cycle. *J Neurosci* 26:12587–12595.
27. Kish LJ, Palmer MR, Gerhardt GA (1999) Multiple single-unit recordings in the striatum of freely moving animals: Effects of apomorphine and D-amphetamine in normal and unilateral 6-hydroxydopamine-lesioned rats. *Brain Res* 833:58–70.
28. Rinzel J, Ermentrout BB (1999) Analysis of neural excitability and oscillations. *Methods in Neuronal Modeling*, eds Koch C, Segev I (MIT Press, Cambridge, MA), 2nd Ed, pp 251–292.
29. Taverna S, Ilijic E, Surmeier DJ (2008) Recurrent collateral connections of striatal medium spiny neurons are disrupted in models of Parkinson's disease. *J Neurosci* 28: 5504–5512.
30. Czubayko U, Plenz D (2002) Fast synaptic transmission between striatal spiny projection neurons. *Proc Natl Acad Sci USA* 99:15764–15769.
31. Koós T, Tepper JM (1999) Inhibitory control of neostriatal projection neurons by GABAergic interneurons. *Nat Neurosci* 2:467–472.
32. Mitzdorf U (1985) Current source-density method and application in cat cerebral cortex: Investigation of evoked potentials and EEG phenomena. *Physiol Rev* 65:37–100.
33. Ryan LJ, Tepper JM, Young SJ, Groves PM (1986) Frontal cortex stimulation evoked neostriatal potentials in rats: Intracellular and extracellular analysis. *Brain Res Bull* 17: 751–758.
34. Tsirogiannis GL, Tagaris GA, Sakas D, Nikita KS (2010) A population level computational model of the basal ganglia that generates parkinsonian Local Field Potential activity. *Biol Cybern* 102:155–176.
35. Jensen O, et al. (2005) On the human sensorimotor-cortex beta rhythm: Sources and modeling. *Neuroimage* 26:347–355.
36. Mitra P, Bokil H (2007) *Observed Brain Dynamics* (Oxford University Press, New York).

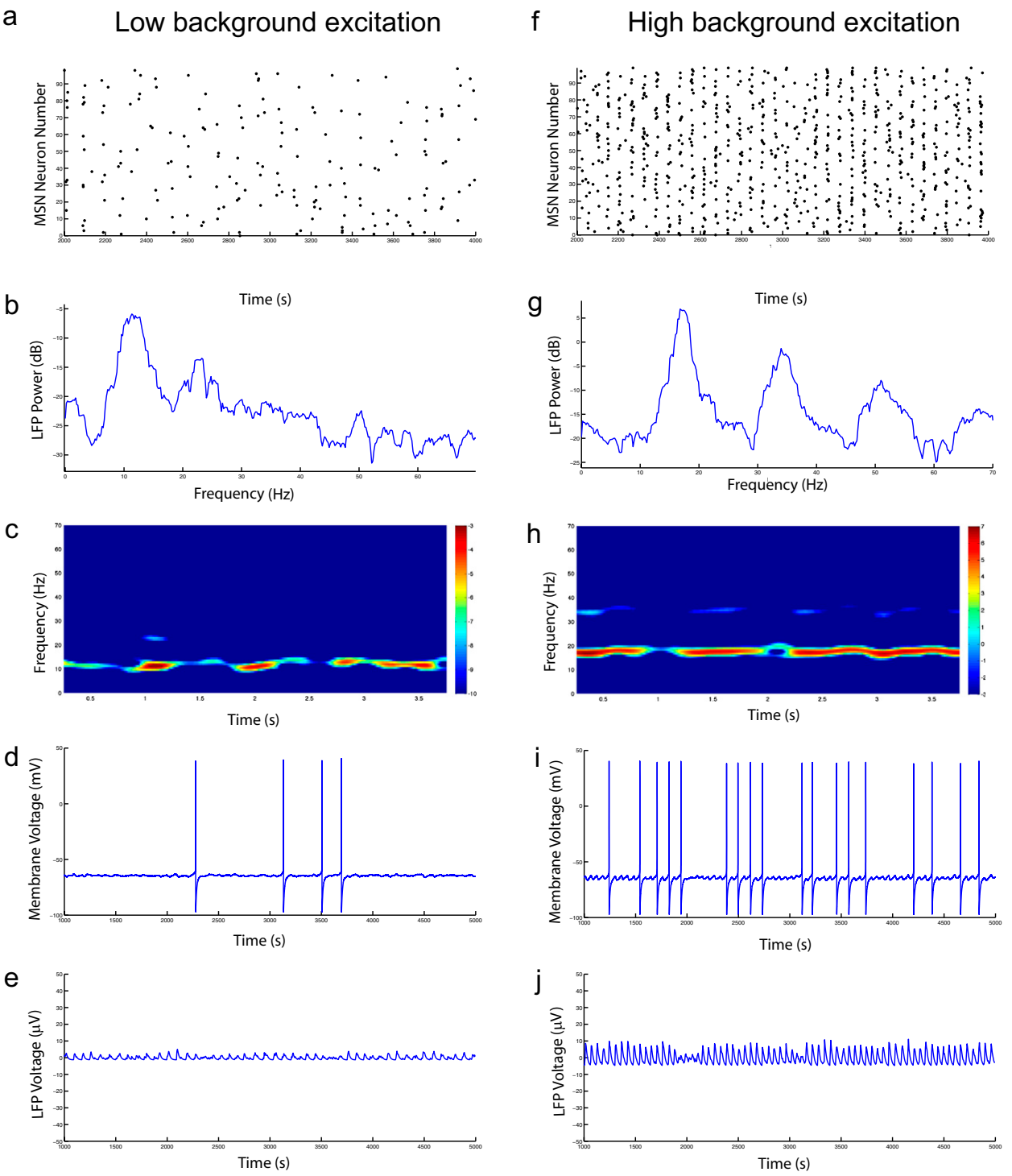

Fig. S1. Some combinations of parameter changes allow for a larger or smaller percentage decrease in $\bar{g}_m$ from the normal to the parkinsonian state. A different combination of parameters [I_{app} = 0.4 μA/cm^2, $\bar{g}_{ii}$ = 0.25 mS/cm^2, $\bar{g}_m$ = 0.34 mS/cm^2(normal), and 0.2 mS/cm^2 (Parkinson's disease)] in our all-to-all connected 100-neuron MSN model gives qualitatively similar results to our original model but with a 41.2% decrease in $\bar{g}_m$ between the normal and the parkinsonian states. *A–E* are taken from the same simulation under normal conditions, and *F–J* are taken from the same simulation under parkinsonian conditions. (*A*) Raster plot of 100 reciprocally connected MSNs under normal non-parkinsonian conditions. The average spiking rate of the MSNs is 0.905 Hz. (*B*) Power spectral density of the model LFP. Spectral power peaks at ∼11.4 Hz. (*C*) Spectrogram of the model LFP. (*D*) Membrane voltage fluctuations from one MSN in the network. (*E*) The model LFP trace under normal conditions contains a low-voltage, waxing and waning beta oscillation. (*F*) Raster plot of 100 reciprocally connected MSNs under parkinsonian conditions. The average MSN spiking rate is 4.11 Hz. (*G*) Power spectral density of the model LFP. Spectral power peaks at ∼16.8 Hz. (*H*) Spectrogram of the model LFP. (*I*) Membrane voltage fluctuations from one MSN in the parkinsonian network. (*J*) The model LFP trace under parkinsonian conditions shows higher voltage oscillations.

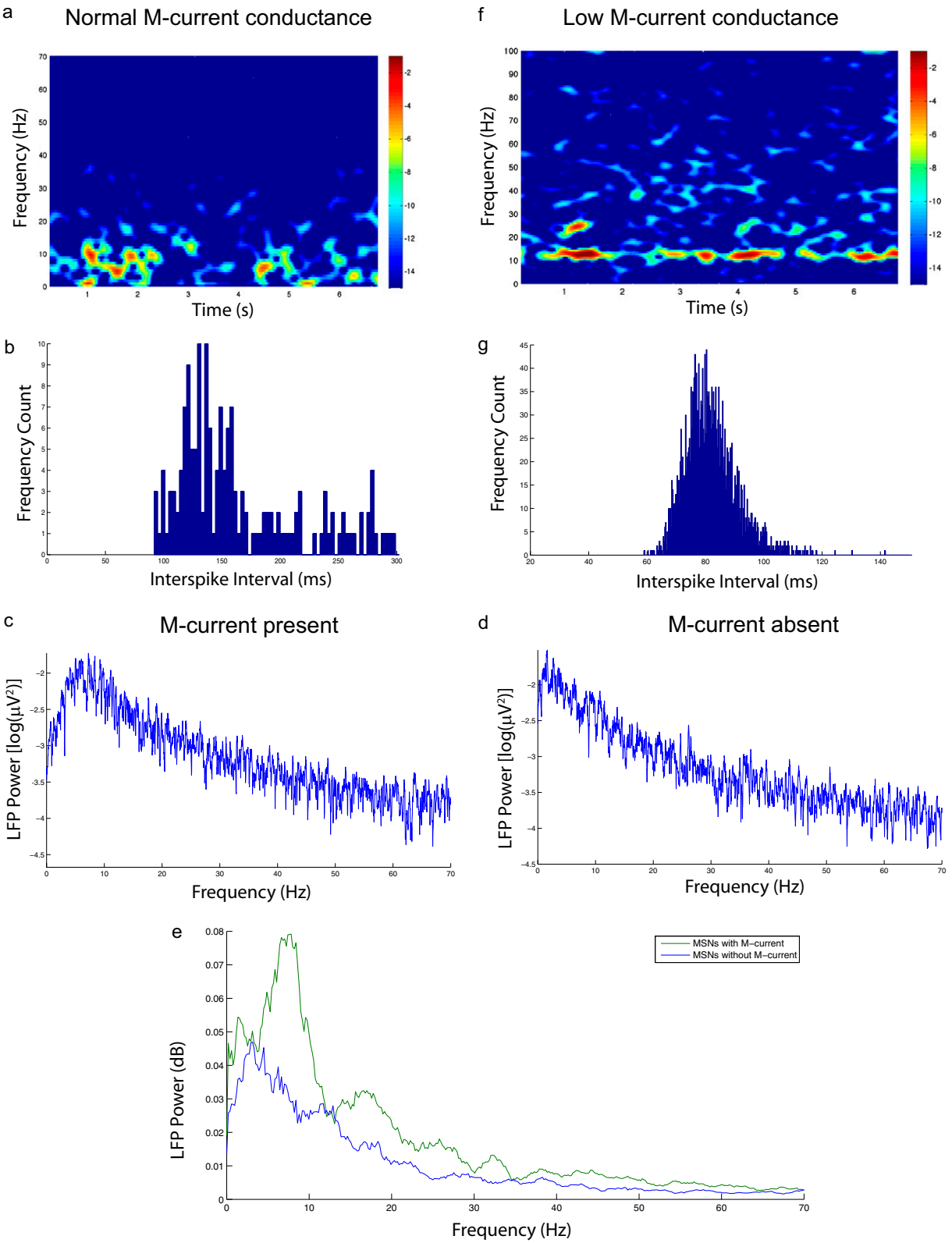

Fig. S2. Low-frequency (8–13 Hz) oscillations remain after removal of all GABAa connections between MSNs. (*A*) Low-frequency beta oscillations in the model LFP from ∼8 to 14 Hz wax and wane throughout a 7-s simulation of 100 unconnected MSNs. Theta (4–7 Hz) and delta (0.5–3 Hz) oscillations are also present (parameters: $\bar{g}_m$ = 1.3 mS/cm^2 and I_{app} = 1.19 μA/cm^2). (*B*) A histogram of the interspike intervals from the 100 MSNs shown in *A*. The histogram peaks between 130 and 138 ms. (*C*) Subthreshold membrane potential oscillations of one MSN contain a 5- to 9-Hz peak in response to Gaussian noise when an M-current is present in the MSN (parameters: $\bar{g}_m$ = 1.3 mS/cm^2 and I_{app} = 1.12 μA/cm^2). These low-frequency oscillations appear to be due to the intrinsic membrane properties of MSNs with M-current. (*D*) The subthreshold membrane potential of one MSN without an M-current does not oscillate at 5–9 Hz. Peak spectral density is at ∼1.65 Hz ($\bar{g}_m$ = 0 mS/cm^2 and I_{app} = 0.09 μA/cm^2). All subthreshold membrane potentials in *C* and *D* were collected over 40 simulated seconds.

Legend continued on following page

(*E*) Power spectral densities averaged over seven 3-s simulations using 100 unconnected model MSNs with an M-current ($\bar{g}_m$ = 1.3 mS/cm^2 and I_{app} = 1.19 μA/cm^2) and without an M-current ($\bar{g}_m$ = 0 mS/cm^2 and I_{app} = 1.1 μA/cm^2). The power peaks near 8 Hz when the M-current is present and around 3 Hz when the M-current is absent. (*F*) Lowering the M-current conductance in the same model as in *A* results in a model LFP oscillation with a peak frequency of 12.2 Hz (parameters: $\bar{g}_m$ = 1.2 mS/cm^2 and I_{app} = 1.19 μA/cm^2). (*G*) A histogram of the interspike intervals from the 100 MSNs in *F*. The histogram peaks at 80 ms.

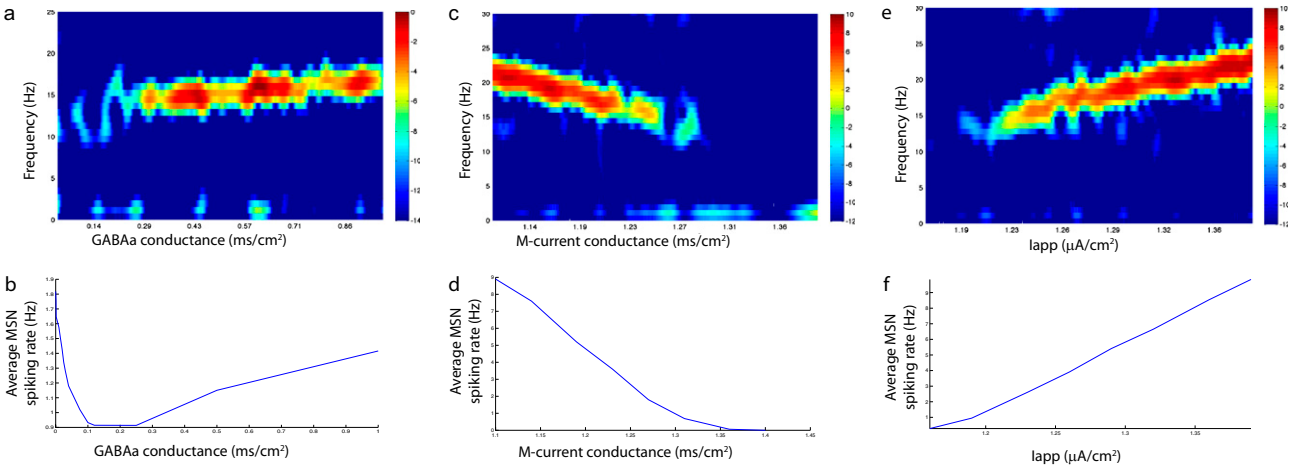

Fig. S3. GABAa conductance, M-current conductance, and background excitation (I_{app}) modulate both the model MSN spiking rate and the peak model LFP power. (*A*) The peak frequency of the beta oscillation changes as a function of the maximal GABAa conductance over the range of GABAa conductances from 0.0001 to 1 mS/cm^2. (*B*) The average MSN spiking rate changes nonlinearly and only slightly as GABAa conductance is increased. (*C*) The peak frequency and power of the beta oscillation decreases as the M-current conductance is increased over the range of 1.1–1.4 mS/cm^2. (*D*) The spiking rate of the MSNs decreases as the M-current conductance is increased. (*E*) The peak frequency of the beta oscillation increases as I_{app} increases over the range of 1.16–1.39 μA/cm^2. (*F*) The spiking rate of the MSNs increases as I_{app} increases. Data points for the spectrograms were recorded for simulations of 7 s duration in a network with all-to-all connections. Parameters were fixed at GABAa conductance = 0.1 mS/cm^2, M-current conductance = 1.3 mS/cm^2, and I_{app} = 1.19 μA/cm^2, if the parameter was not varied in the simulation.

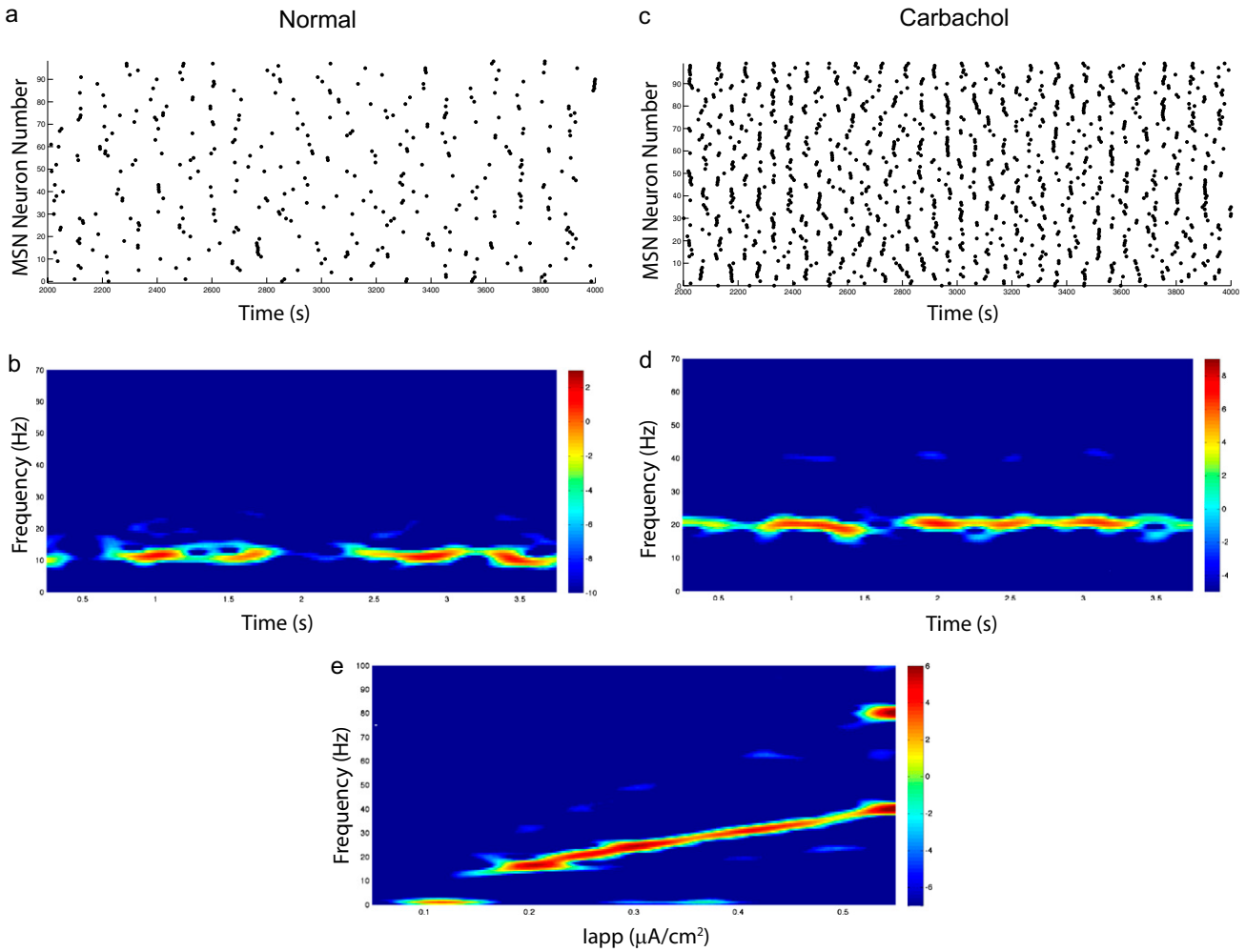

Fig. S4. Network model of FS interneurons can also produce 8- to 30-Hz oscillations. (*A*) Raster plots of 100 FS interneurons interconnected with all-to-all GABAa synapses and electrical synapses to their two nearest neighbors under a low-excitation state (normal; I_{app} = 0.15 μA/cm^2). The raster plot shows some minor patterning of the FS interneuron spike times. The average spiking rate of the FS interneurons is 2.0 Hz. (*C*) The same 100 FS interneuron network as in *A* in the high excitation state (carbachol; I_{app} = 0.25 μA/cm^2). The raster plot shows more distinct patterning of the FS interneurons. The average spiking rate increases to 6.8 Hz. (*B* and *D*) Spectrograms of the model LFP under (*B*) the low-excitation state, showing a waxing and waning oscillation around 11.3 Hz, and (*D*) the high-excitation state, showing a slightly more persistent oscillation around 20.1 Hz. (*E*) Spectrogram of the model LFP from the FS interneuron network shows that the peak frequency of the oscillatory activity tends to increase as the background excitation (I_{app}) is increased. Higher values of I_{app} can give peak frequencies in the gamma frequency band.

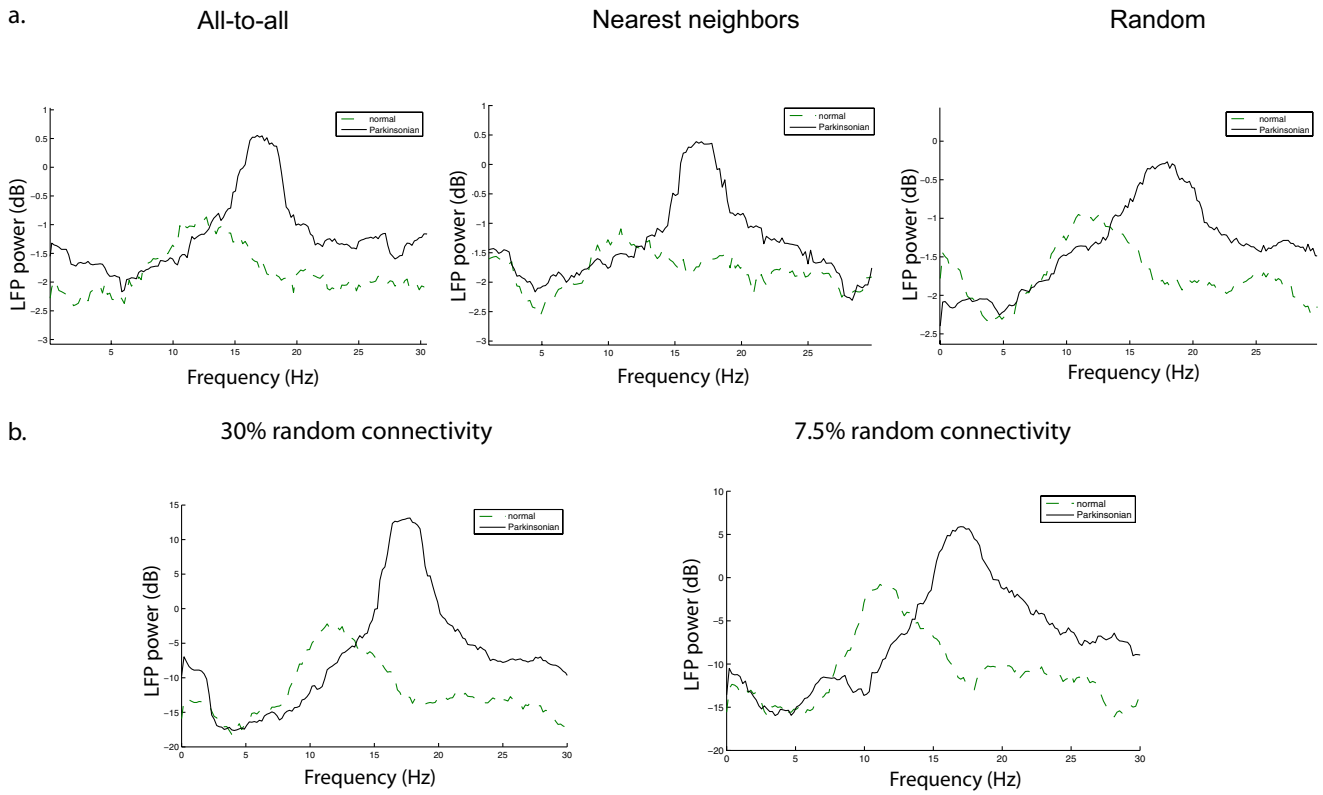

Fig. S5. Model results are largely invariant to network connectivity and network size. (*A*) Model LFPs from striatal networks of 100 MSNs connected all-to-all, to nearest neighbors, and randomly under normal and parkinsonian conditions. (*B*) Model LFPs from striatal networks of 400 MSNs with 30% random connections and 7.5% random connections under normal and parkinsonian conditions.

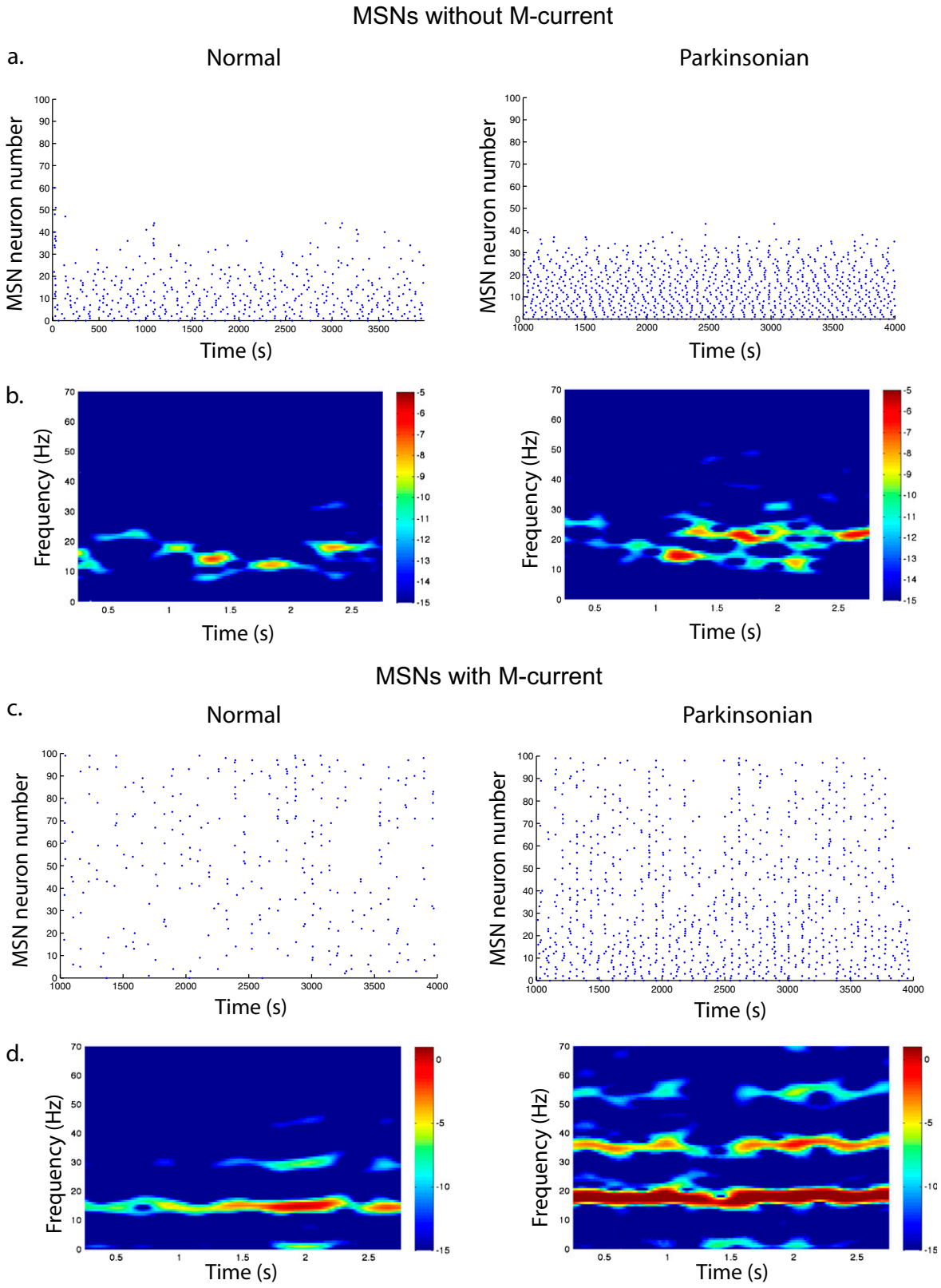

Fig. S6. MSN network is robust to heterogeneity if MSNs have an M-current. (*A*) Raster plots from 100 MSNs without M-current connected all-to-all with heterogeneity of the maximal GABAa conductance under normal and parkinsonian conditions. (*B*) Spectrograms from the simulations that produced the raster plots in *A*. (*C*) Raster plots from 100 MSNs with M-current and connected all-to-all with heterogeneity of the maximal GABAa conductance under normal and parkinsonian conditions. (*D*) Spectrograms from the simulations that produced the raster plots in *C*.

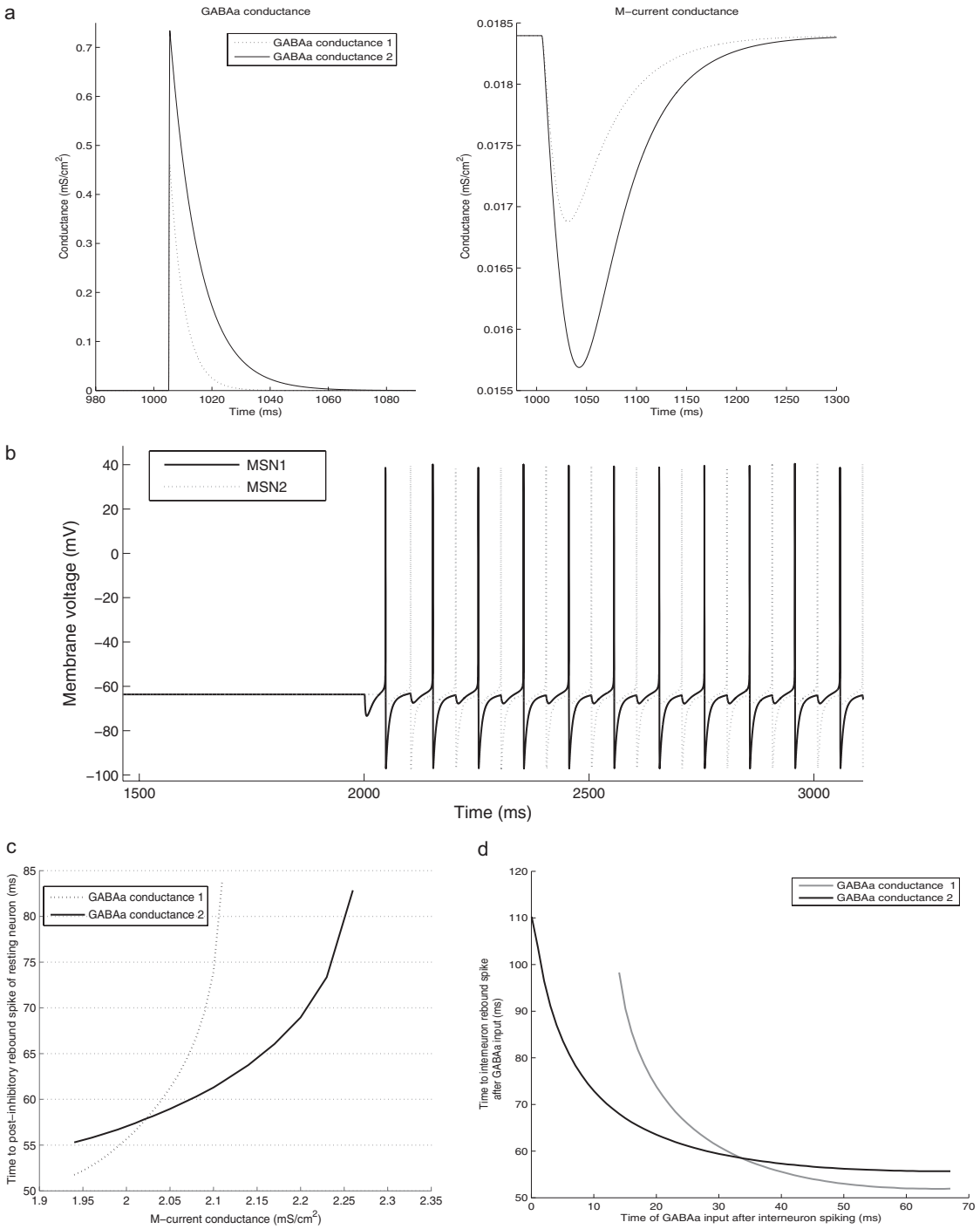

Fig. S7. Mechanism of GABAa-induced excitation in neurons with an M-current. (*A*) Increasing the GABAa conductance decreases the M-current conductance in a simulated neuron: $\bar{g}_{ii} = 0.165$ mS/cm^2, τ_i = 5 ms for GABAa conductance 1, $\bar{g}_{ii} = 0.25$ mS/cm^2, and τ_i = 10 ms for GABAa conductance 2. (*B*) Simulation results of two MSNs reciprocally connected with GABAa synapses. Both neurons are quiescent until MSN1 receives external inhibition at 2,000 ms, causing it to rebound spike and enabling the formation of an antisynchronous rhythm between the two MSNs in the beta frequency range (20 Hz). (*C*) Simulation results showing that the time to rebound spiking after GABAa inhibition is dependent on both the M-current conductance and the GABAa current conductance. GABAa conductance 1 and 2 are as defined in *A*. (*D*) Simulation results show that the time to rebound spiking after a previous spike is dependent on the GABAa conductance. GABAa conductance 1 and 2 are as defined in *A*. *A*–*D* have been modified from ref. 1.

1. McCarthy MM, Brown EN, Kopell N (2008) Potential network mechanisms mediating electroencephalographic beta rhythm changes during propofol-induced paradoxical excitation. *J Neurosci* 28:13488–13504.